JOURNAL OF GEOPHYSICAL RESEARCH, VOL. 111, B09410, doi:10.1029/2005JB004158, 2006

Intrinsic elasticity of a textured transversely isotropic muscovite aggregate: Comparisons to the seismic anisotropy of schists and shales

Pavlo Y. Cholach[1,2] and Douglas R. Schmitt[1]

Received 9 November 2005; revised 2 June 2006; accepted 22 June 2006; published 30 September 2006.

[1] The anisotropic properties of phyllosilicate rocks are investigated through the modeling of the pore-free "intrinsic" elasticity of a textured muscovite aggregate. The elastic constants were calculated for textures, as defined using orientation distribution functions (ODFs), ranging from perfectly aligned to completely random. The ODFs were described using a Gaussian distribution, the width of which is controlled by the standard deviation of the orientations of the crystal *c* axis with respect to the sample foliation plane under the assumption that the sample has hexagonal (transversely isotropic) symmetry. The values were obtained using the widely used Voigt-Reuss-Hill averaging techniques as well as the geometric mean average (GMA). The GMA is more physically meaningful in that it requires that the elastic constants determined in either the stiffness or the compliance domains be invertible. Comparisons between these different averages indicate that, strictly, the Voigt and Reuss values do not necessarily provide the limiting bounds as is expected for the isotropic case. Despite this, some characteristics of the elastic wave *P* wave anisotropy are only weakly dependent on the averaging procedure employed. The calculated elastic constants are converted to the anisotropic ε, δ, and γ parameters in order to allow for comparison to existing measurements in the literature. However, these "intrinsic" results are not intended to provide a measure of the properties of phyllites per se but to provide a reference against which more sophisticated models that incorporate porosity, layering, and composition may be constructed.

Citation: Cholach, P. Y., and D. R. Schmitt (2006), Intrinsic elasticity of a textured transversely isotropic muscovite aggregate: Comparisons to the seismic anisotropy of schists and shales, *J. Geophys. Res.*, *111*, B09410, doi:10.1029/2005JB004158.

1. Introduction

[2] Phyllosilicate minerals such as clays and micas occur in rocks from the uppermost mantle to the Earth's surface. A large fraction of sedimentary basins are filled with clays. Micas are a major component of most metamorphic rocks and dominate in slates and schists. The mica phlogopite is considered as an important carrier of water in both subduction zones and mantle wedges. It is seen in mantle xenoliths in ultrahigh metamorphic materials [e.g., *van Roermund et al.*, 2002; *Hearn*, 2004; *Chen et al.*, 2005] and is stable to pressure and temperature (P/T) conditions expected at depths to at least 150 km [e.g., *Sudo and Tatsumi*, 1990; *Tronnes*, 2002]. An understanding of the anisotropy of the upper mantle and crust requires that the role of phyllosilicate minerals be considered particularly with regard to the influence of tectonic straining on texture.

[3] Ignoring anisotropy has a number of consequences. In active seismic images estimates of both the depth and the lateral position of a subsurface feature will be in error [e.g., *Banik*, 1984; *Godfrey et al.*, 2002] particularly if the symmetry axes of the rocks are tilted [*Vestrum et al.*, 1999; *Okaya and McEvilly*, 2003]. At a crustal scale, anisotropy in such rocks will also influence the interpretation of reflection and refraction profiles and could contribute significantly to SKS shear wave splitting delay times [e.g., *Ji and Salisbury*, 1993; *Barruol and Mainprice*, 1993; *Godfrey et al.*, 2000; *Okaya et al.*, 2004; *Cholach et al.*, 2005] although field observations over areas in which the crust is expected to be anisotropic have been mixed [*Vergne et al.*, 2003; *Pulford et al.*, 2003]. Consequently, having knowledge of the range of anisotropy that might be anticipated from these phyllosilicate aggregate rocks would provide a useful tool to assist in the interpretation of seismic observations.

[4] Aside from their abundance, the large anisotropy of the phyllosilicate single crystals and the propensity of their aggregate to be textured both contribute to the overall anisotropy of many rocks. In this contribution the issue of the origin of seismic anisotropy of phyllosilicate rich rocks is partially addressed by modeling of their intrinsic aggregate elastic properties. "Intrinsic" here is taken to mean the elastic anisotropy due solely to the averaging of the elastic properties of the constituent minerals as controlled by their texture; quantitatively described by an orientation distribution function (ODF). The geometric mean averaging (GMA) procedure is applied to a range of axially symmetric aggregate textures from completely random (i.e., isotropic)

[1] Institute for Geophysical Research, Department of Physics, University of Alberta, Edmonton, Alberta, Canada.
[2] Now at BP Canada Energy Company, Calgary, Alberta, Canada.

0148-0227/06/2005JB004158$09.00

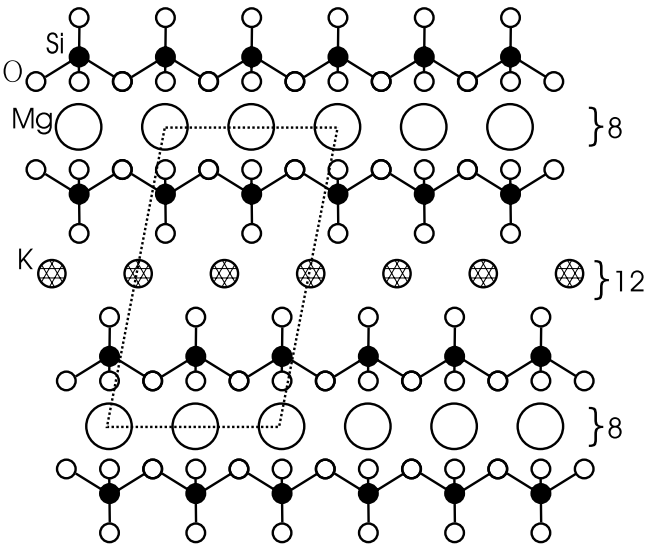

Figure 1. Simplified atomic view along the planes of muscovite showing octohedrally coordinated Mg or Al cations and 12 coordinated K cations separating silicate sheets. The unit cell is delineated by a dashed parallelogram.

to completely aligned (i.e., anisotropy of the single crystal), these new calculations are compared with the more traditional and normally employed Voigt-Hill-Reuss methods. Parameterizations of the anisotropy are then compared with existing measurements on phyllites in the literature. The evolution of the anisotropy with texture and the comparison to laboratory observations provides insight into some of the factors controlling the elastic anisotropy of these rocks. This study provides measures of the elasticity of a pore free solid matrix that can be used as a baseline for more complex models incorporating porosity, layering, or other mineral phases. The paper first outlines the current state of knowledge of phyllosilicate mineral elasticity, defines the ODF, and reviews the pertinent literature before developing and applying the GMA method for this case.

2. Elasticity of Micas and Clays

[5] Phyllosilicates are some of the most elastically anisotropic crystals. X-ray diffraction studies allow the linear compressibilities of single mica crystals to be determined under high-pressure hydrostatic compression. The ratio between the linear compressibilities measured parallel and perpendicular to the silicate sheets can exceed 4 [e.g., *Comodi et al.*, 2004]. The longitudinal wave anisotropy ($A_p = [V_p^{\max} - V_p^{\min}]/V_p^{mean} \times 100\%$) in single crystal muscovite is 56.8% [*Alexandrov and Ryzhova*, 1961] while in a biotite the speed of the two birefringent shear waves propagating parallel to the strong [001] cleavage differ by a factor of nearly 3.7.

[6] Some of the more important phyllosilicate minerals include the micas muscovite, phlogopite, and biotite and the clay illite [e.g., *Deer et al.*, 1964]. These minerals share many of the same structural characteristics [see *Vaughan and Guggenheim*, 1986; *Putnis*, 1992] with the basic building block (Figure 1) consisting of sheets of linked $(Si,Al)O_4$ tetrahedra bounding a layer of octahedrally coordinated cations (e.g., Mg in pure end-member muscovite) with two thirds of these sites filled with trivalent cations. The resulting lamina has a net negative charge, which is then balanced by layers of twelvefold coordinated cations (e.g., K in pure end-member muscovite). At the level of a single lamina, illite differs from muscovite only by the substitution of different elements into the atomic sites. There are fewer interlayer cations; this leads to less structured stacking and weaker interatomic forces between the layers. In biotite and its end-member phlogopite all of the octahedral coordinated sites are filled with divalent cations and these result in a different trioctahedral structure. Despite the minor structural differences, these phyllosilicate minerals have similar unit cell dimensions (Table 1).

[7] The elastic properties of muscovite, phlogopite, and a biotite have been directly measured and modeled (see references in Table 2). This work suggests that although these minerals usually have monoclinic symmetry, their elasticity properties are nearly axially symmetric with respect to the *c* axis and for practical purposes they may be considered to have hexagonal symmetry. Clay crystals typically have submicron dimensions; direct measurements are difficult and their moduli have to date only been inferred (Table 2). The elastic stiffnesses of illite are not yet known; and it is often assumed that muscovite's elastic properties may instead be employed [e.g., *Tosaya*, 1982; *Katahara*, 1996; *Sayers*, 1994]. The similarity of both the moduli between the various crystals and of their atomic structures suggests that the elastic values of muscovite are likely representative of those for illite. However, the minor discrepancies between the different measurements for muscovite suggest that much experimental work still needs to be carried out.

3. Texture and the Orientation Distribution Function

[8] The second factor in relation to phyllite anisotropy is that phyllosilicates are usually preferentially oriented with respect to the rock's textural elements; indeed, it is the relative orientations of the phyllosilicate minerals that often

Table 1. Characteristics of Representative Mica and Clay Minerals

Phyllosilicate	Stoichimetry[a]	Unit Cell Dimensions, Å[a]			Symmetry[a]
		a	b	c	
Muscovite	$K_2Al_4[Si_6Al_2O_{20}](OH,F)_2$	5.19	9.04	9.98	monoclinic
Illite	$K_{1\text{-}1.5}Al_4\ [Si_{7\text{-}6.5}Al_{1\text{-}1.5}O_{20}](OH)_4$	5.2	9.0	9.95	monoclinic
Phlogopite	$K_2(Mg,Fe^{+2})_6\ [Si_6Al_2O_{20}]\ (OH,F)_4$	5.314	9.204	10.314	monoclinic
Biotite	$K_2(Mg,Fe^{+2})_{6\text{-}4}(Fe^{+3},Al,Ti)_{0\text{-}2}\ [Si_{6\text{-}5}Al_{2\text{-}3}O_{20}]O_{0\text{-}2}(OH,F)_{4\text{-}2}$	5.3	9.2	10.2	monoclinic

[a] *Deer et al.* [1964].

Table 2. Elastic Properties of Micas and Clays

		Bulk Modulus K_o and Stiffnesses C_{ij}, GPa									
Mineral	Density, kg/m^3	K_o	C_{11}	C_{22}	C_{33}	C_{44}	C_{55}	C_{66}	C_{12}	C_{13}	C_{23}
Muscovite[a]	2844	58.2	184.3	178.4	59.1	16.0	17.6	72.4	48.3	23.8	21.7
Muscovite[b]	2790	52.2	178.0	178.0	54.9	12.2	12.2	67.8	42.4	14.5	14.5
Muscovite[c]	-	-	168.0	217.2	47.8	10.2	18.2	56.9	-	-	-
Muscovite[c]	-	-	170.8	203.2	47.9	11.0	17.6	54.6	-	-	-
Muscovite[d]	-	49.0	-	-	-	-	-	-	-	-	-
Muscovite[e]	-	54.0	-	-	-	-	-	-	-	-	-
Muscovite[f]	-	51–58	-	-	-	-	-	-	-	-	-
Muscovite[g]	-	57 ± 3	-	-	-	-	-	-	-	-	-
Muscovite[h]	-	62 ± 2	-	-	-	-	-	-	-	-	-
Biotite[i]	3050	50.5	186.0	186.0	54.0	5.8	5.8	76.8	32.4	11.6	11.6
Phlogopite[b]	2800	54.8	179.0	179.0	51.7	5.6	5.6	73.3	32.4	25.8	25.8
Phlogopite[b]	2820	49.7	178.0	178.0	51.0	6.5	6.5	73.9	30.2	15.2	15.2
Phlogopite[i]	-	49.7 ± 0.2	-	-	-	-	-	-	-	-	-
Phlogopite[j]	-	58.5	-	-	-	-	-	-	-	-	-
Phlogopite[k]	-	54 ± 2	-	-	-	-	-	-	-	-	-
Illite[l]	2706	60.1	-	-	-	-	-	-	-	-	-
Kaolinite[m]	-	7.4	-	-	-	-	-	-	-	-	-
"Clays"[n]	-	21.4	-	-	-	-	-	-	-	-	-
Smectite[o]	-	5.75	-	-	-	-	-	-	-	-	-
Kaolinite[o]	-	11	-	-	-	-	-	-	-	-	-
"Clays"[n]	-	21.4	-	-	-	-	-	-	-	-	-
Clay[p]	-	12.5	-	-	-	-	-	-	-	-	-
Clay[q]	-	22.9	-	-	-	-	-	-	-	-	-
Clay[r]	2730	-	85.6	85.6	65.5	29.7	29.7	24.6	-	-	-
Clay[s]			38.1	38.1	18.8	-	13.8	9.5	-	-	-

[a]Measured using Brillouin scattering by *Vaughan and Guggenheim* [1986]. These authors note that this material has nearly hexagonal symmetry with small monoclinic stiffness values $C_{15} = -2.0$ GPa, $C_{25} = 3.9$ GPa, $C_{35} = 1.2$ GPa, and $C_{46} = 0.5$ GPa.

[b]Measured by ultrasonic pulse transmission on large single crystals by *Alexandrov and Ryzhova* [1961] as reported by *Simmons and Wang* [1971] with $C_{66} = (C_{11} - C_{12})/2$ under the presumption of hexagonal symmetry within experimental uncertainty. See also *Katahara* [1996] and *Nishizawa and Yoshino* [2001]. Bulk modulus K_o is the Hill average of the Voigt and Reuss bounds for an isotropic aggregate as calculated by *Simmons and Wang* [1971].

[c]Derived in atomistic simulation on $KAl_{2(oct)}Al_{(tet)}Si_3O_{10}(OH)_2$ by *Purton et al.* [1997]. The third and fourth rows are for their hybrid and ordered models, respectively.

[d]For synthetic muscovite $(Na_{0.07}K_{0.90}\ Ba_{0.01})(Al_{1.84}Ti_{0.04}Fe_{0.07}Mg_{0.04})(Si_{3.02}Al_{0.98})O_{10}(OH)_2$ using X-ray diffraction in diamond anvil cell by *Comodi and Zanazzi* [1995]. K_o is zero-pressure bulk modulus determined from fit of third-order Birch-Murnaghan equation of state.

[e]For synthetic muscovite $(Na_{0.37}K_{0.60})(Al_{1.84}Ti_{0.02}\ Fe_{0.10}Mg_{0.06})(Si_{3.03}Al_{0.97})O_{10}(OH)_2$ using X-ray diffraction in diamond anvil cell by *Comodi and Zanazzi* [1995].

[f]For natural muscovite (monoclinic phengite, $K_{0.96}Na_{0.01}Al_{1.44}Mg_{0.56}(Si_{3.59}Al_{0.41})$-$O_{10}(OH_{1.93},F_{0.07})$) using X-ray diffraction in a Paris-Edinburgh cell) by *Pavese et al.* [1999]. The range of values of the bulk modulus arises from the comparison of a series of different finite strain equations of state to the observed compressions.

[g]For synthetic high-silica muscovite (monoclinic phengite, $K(Al_{1.2}1Mg_{0.75}Fe_{0.04})(Al_{0.19}Si_{3.81})O_{22}(OH_{1.2}F_{0.8})$) by X-ray diffraction reported by *Smyth et al.* [2000]. Bulk modulus determined from fit of third-order Birch-Murnaghan equation of state.

[h]For the same synthetic material as in footnote e, but with trigonal symmetry reported by *Smyth et al.* [2000].

[i]For natural phlogopite $(K_{0.99(1)}Na_{0.020(3)})$ $1.01(Mg_{2.73(6)}Fe_{0.15(1)}Al_{0.06(1)}Ti_{0.02(3)})$ $2.96(Al_{1.07(2)}Si_{2.93(3)})$ $4O_{10}(OH)_2$ by X-ray diffraction reported by *Pavese et al.* [2003]. Bulk modulus determined from third-order fit of data to Birch-Murnaghan equaton of state.

[j]For natural phlogopite by X-ray diffraction in a diamond anvil cell by *Hazen and Finger* [1978].

[k]For natural phlogophite $([(K_{0.91}Na_{0.02}Ba_{0.03})(Fe_{0.652} + Fe_{0.1633} + Al_{0.123}Mg_{1.81}Ti_{0.149})Si_{2.708}Al_{1.292}O_{10}OH_{1.725}F_{0.175}])$ by X-ray diffraction in a diamond anvil cell by *Comodi et al.* [2004].

[l]For illite (sample IMt2) determined by measurements of density and of ultrasonic longitudinal and shear wave velocities on a series of epoxy-clay composites by *Wang et al.* [1998]. Bulk modulus is the Hashin-Shtrikman average.

[m]For kaolinite (dickite) with atomic force microscopy by *Prasad et al.* [2002]. This value is calculated from the given Young's modulus of $E = 6.2 \pm 1.0$ GPa measured in the C_{11} direction according to $K = E/3(1 - 2\nu)$ with Poisson's ratio $\nu = 0.3$.

[n]For generic clays as suggested by *Berge and Berryman* [1995] based on the compilations of laboratory measurements by *Castagna et al.* [1985].

[o]From ultrasonic velocity measurements on porous clay aggregates by *Vanorio et al.* [2003].

[p]Inferred from velocity measurements on a water-clay composite assuming isotropy by *Marion et al.* [1992].

[q]Inferred from *Marion et al.*'s [1992] measurements using an isotropic self-consistent approximation by *Hornby* [1995].

[r]Inferred by *Vernik and Liu* [1997] in their calculations of the anisotropy of shales consisting of a mix of kerogen and clay, moduli determined from velocities and densities provided.

[s]Estimated by *Sayers* [2005] for a clay domain from the shale measurements of *Jones and Wang* [1981] under the assumption that his Legendre coefficients were 60% of the maximum values possible (i.e., for a single crystal).

delineate the texture. In sediments not subject to tectonic straining, this orientation is possibly linked to the conversion of smectite to illite [*Sintubin*, 1994a; *Ho et al.*, 1999; *Aplin et al.*, 2003] or to low-grade metamorphism and recrystallization of grains [e.g., *Sintubin*, 1994b; *Jacob et al.*, 2000]. The textures of such rocks are visually rotationally symmetric with respect to the bedding or foliation planes and they are consequently expected to be transversely isotropic [e.g., *Kaarsberg*, 1959; *Hornby*, 1995]. Oriented electron micrographs of a shale (Figure 2) illustrate this overall axial symmetry with the planes of the clay platelets primarily horizontally oriented. However, nonlithostatic tectonic deformation produces orthorhombic texture [e.g., *Oertel*, 1983; *Sintubin*, 1994b] consistent with long-standing deformation models. *O'Brien et al.* [1987] have found even more complex deformation in a series of X-ray

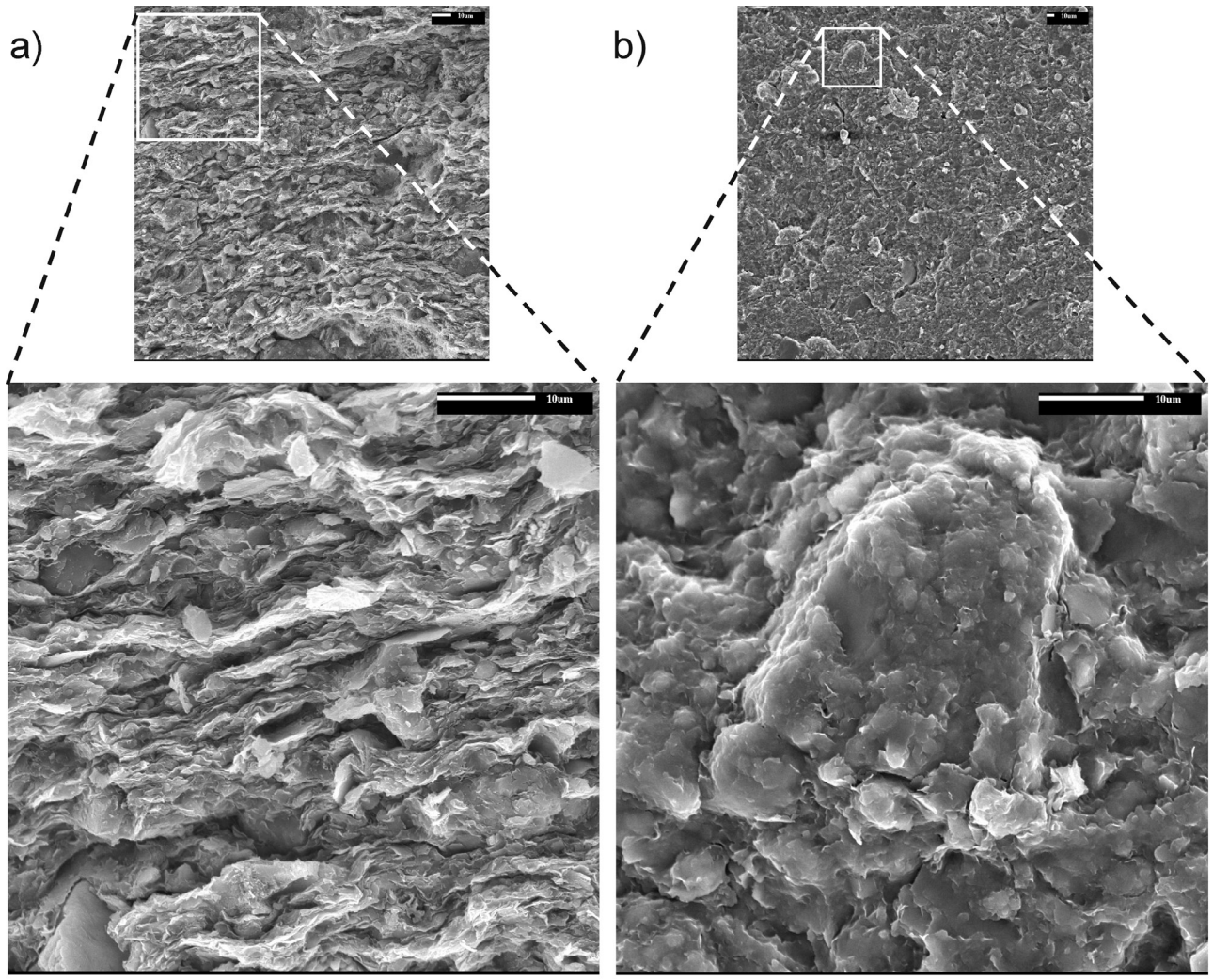

Figure 2. SEM images of Colorado Shale from the Cold Lake area of Alberta, Canada: (a) section perpendicular to the bedding plane and (b) section parallel to the bedding plane. Observed strong preferred orientation of clay particles directly correlates with lattice preferred orientation of clay minerals (see text for details). Average size of clay platelets is several microns. Images are shown only to illustrate the mineralogic textures of such shales.

goniometry measurements on metamorphic phyllites. The degree to which these highly anisotropic minerals are preferentially aligned within the aggregate rock contributes greatly to the structure's seismic anisotropy [e.g., *Brocher and Christensen*, 1990; *Kern and Wenk*, 1990; *McDonough and Fountain*, 1993; *Burlini and Fountain*, 1993; *Mainprice and Humbert*, 1994; *Godfrey et al.*, 2000; *Weiss et al.*, 1999; *Takanashi et al.*, 2001; *Cholach et al.*, 2005], and as such their elastic anisotropy is important in seismic investigations of the crust and upper mantle at many scales.

[9] Textures are quantitatively described with an orientation distribution function (ODF) $f(g)$ [*Bunge*, 1982], where $g = \{\varphi_1, \Phi, \varphi_2\}$ is the orientation domain consisting of the three Euler angles [cf. *Morse and Feshbach*, 1953]. The angles g describe the orientation of the individual mineral's coordinate reference frame $x_i = (x_1, x_2, x_3)$ (Figure 3b) with that for the aggregate $X_j = (X_1, X_2, X_3)$ (Figure 3c). Three consecutive rotations of an initially misaligned single crystal coordinate system x_i by Euler angles $\{\varphi_1, \Phi, \varphi_2\}$ bring it to coincide with X_j. X_j is defined such that the X_1X_2 plane coincides with the foliation or bedding plane. The lineation direction, should it exist, defines X_1. Axis X_3 is normal to the foliation plane. For the transversely isotropic (i.e., axially symmetric around X_3) aggregate studied here there is no lineation and the X_1 and X_2 directions lie arbitrarily within the foliation or bedding plane (as will be the case here).

[10] Such information is usually obtained from thin section microscopy or X-ray, neutron, and electron (EBSD) diffraction techniques [e.g., *Ullemeyer et al.*, 2000] or estimated from analysis of micrographs [e.g., *Hornby et al.*, 1994]. The choice of the texture determination technique depends on the rock type and the purpose of the investigation. *Ullemeyer et al.* [2000] suggested that so-called "statistical" or "volume" type texture determination techniques, such as X-ray or neutron diffraction, are most suitable for bulk texture determination and calculations of the elastic properties of rocks. *Takanashi et al.* [2001],

O'Brien et al. [1987], *Sintubin* [1994a, 1994b], and *Mainprice and Humbert* [1994] give numerous examples of phyllite ODFs in slates and shales.

[11] The number of the pole figures required to fully describe an ODF, in general, depends on the symmetries of both the constituent mineral and the overall rock sample. Here, the mineral is also assumed to be transversely isotropic and as such the $f(g)$ depends only on the single Euler angle Φ; and only one pole diagram is necessary to describe the orientation statistics.

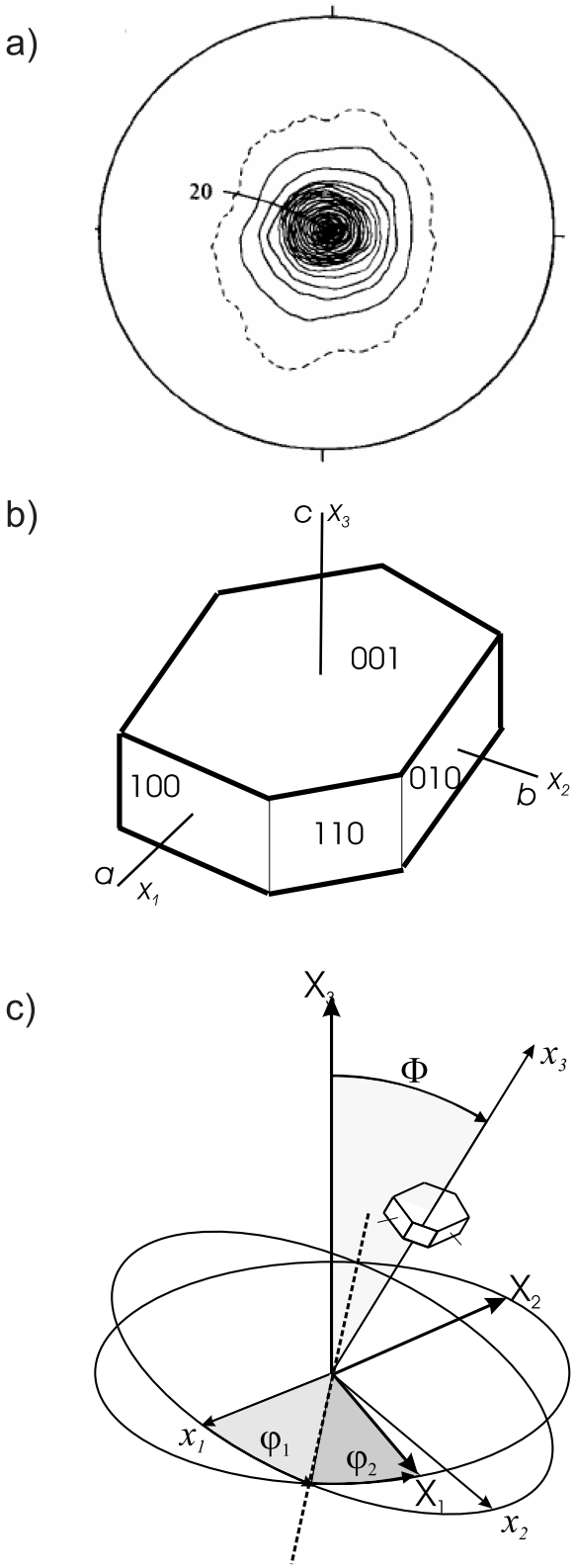

Figure 3. (a) Example of pole figure (lower hemisphere equal-area projection onto the foliation plane) for a mica in a slate obtained by *Sintubin et al.* [1995], with permission from Elsevier. Contour intervals are expressed in terms of multiples of a random distribution with the dashed contour equal to 0.5 and each continuous line contour equal to 1. (b) Individual mineral coordinate reference frame (x_1, x_2, x_3). (c) Relation between mineral (x_1, x_2, x_3) and aggregate (X_1, X_2, X_3) coordinate frames used to describe the orientation of a given mineral using the Euler angles $g = \{-\pi \leq \varphi_1 \leq \pi, 0 \leq \Phi \leq \pi, -\pi \leq \varphi_2 \leq \pi\}$. $X_1 - X_2$ is the foliation or bedding plane, and the X_1 axis defines the lineation if it exists.

4. Earlier Studies on Phyllitic Rocks

4.1. Shales

[12] Since the pioneering work of *Kaarsberg* [1959] shale elasticity has been extensively investigated both theoretically [*Hornby et al.*, 1994; *Sayers*, 1994; *Schoenberg et al.*, 1996; *Sayers*, 1999; *Jakobsen et al.*, 2003], and in the laboratory [*Podio et al.*, 1968; *Jones and Wang*, 1981; *Vernik and Nur*, 1992; *Vernik and Liu*, 1997; *Johnston and Christensen*, 1995; *Hornby*, 1998; *Jakobsen and Johansen*, 2000; *Wang*, 2002; *Domnesteanu et al.*, 2002]. These studies demonstrated that anisotropy is a feature of seismic wave propagation in the majority of shales. The anisotropic behavior of shales was also observed in a variety of seismic field observations [e.g., *Jolly*, 1956; *White et al.*, 1983; *Winterstein and Paulsson*, 1990; *Miller et al.*, 1994; *Kebaili and Schmitt*, 1996; *Leslie and Lawton*, 1999; *Leaney et al.*, 1999]. The significant lithological and compositional variability is responsible for variations in the magnitude of shale anisotropy [*Banik*, 1984; *Jakobsen and Johansen*, 2000; *Wang*, 2002] with the coefficient of anisotropy for compressional wave ($A(V_p) = (V_p^{\max} - V_p^{\min})/V_p^{mean} \times 100\%$) exceeding 40% in some cases [cf. *Johnston and Christensen*, 1995]. Their work also suggests that these rocks are axially symmetric with respect to the bedding plane; and that they must be elastically transversely isotropic. However, a caveat placed on the last statement is that many of the existing measurements are simplified by beginning with the assumption that the rock is transversely isotropic.

[13] The microstructure of shales leading to this anisotropy has been considered in a variety of ways. A number of these studies rely on the anisotropy induced by layering and do not include the full elasticity of the platy minerals. For example, *Vernik and Nur* [1992] applied *Backus* [1962] long-wavelength theory to average the properties of a composite medium consisting of isotropic layers of illite and kerogen in an attempt to explain ultrasonic observations of strong anisotropy in source rock shales. *Hornby et al.* [1994] used the combination of the self-consistent (SCA) [*Kröner*, 1958] and the differential effective medium (DEM) [e.g., *Sheng and Callegari*, 1984] approximations to provide an estimate of the elasticity of a shale domain (i.e., a perfectly aligned clay-fluid layered composite), an ensemble of which were then averaged according to a statistical

measures of the relative orientation of clay platelets as determined from electron micrographs of a shale. Despite ignoring the anisotropic properties of the crystal itself, their calculated elastic constants were almost identical to those obtained from ultrasonic measurements on Cretaceous shales by *Jones and Wang* [1981]. *Schoenberg et al.* [1996] invoked a simplified three-parameter transversely isotropic (TI) medium to model shale anisotropy. Their initial model is based on the long-wavelength approximation of stiffened media consisting of two interchangeable, infinitely thin isotropic layers [*Schoenberg and Muir*, 1989]. Most of the calculated elastic constants of this simplified transversely isotropic medium, with exception of C_{33}, are in reasonable agreement with experimental values.

[14] Despite these advances, there remains significant ambiguity in the models with respect to the in situ sources of seismic anisotropy. Mineralogical texture has been semiquantitatively linked to shale anisotropy in a correlative sense using diffracted X-ray intensities in only two studies [*Kaarsberg*, 1959; *Johnston and Christensen*, 1995] and by clay orientation statistics from electron microscopy in another [*Hornby*, 1995]. The seismic anisotropy in shales is influenced by several factors, including the preferred orientation (texture) of clay platelets [*Kaarsberg*, 1959; *Tosaya*, 1982; *Sayers*, 1994; *Johnston and Christensen*, 1995], alternation of fluid-filled collinear cracks with clay platelets [*Vernik and Nur*, 1992; *Hornby et al.*, 1994], microcracks [*Vernik*, 1993; *Vernik and Liu*, 1997], fine layering [*Schoenberg et al.*, 1996], fluid-filled porosity [*Hornby*, 1998], and stress-induced anisotropy [*Sayers*, 1999]. A combination of several of these factors [e.g., *Jakobsen et al.*, 2003] is required to fully describe shale anisotropy.

[15] The only studies that have explicitly considered clay mineral orientation statistics in shales are those of *Sayers* [1993, 1994], who modeled the properties of textured muscovite aggregates intended to identify the textural parameters responsible for anisotropic velocity variations in shales. *Sayers* [1994] assumed that *Alexandrov and Ryzhova*'s [1961] value for muscovite (Table 2) appropriately represent those of illite. The Voigt approximation of uniform strain of shale aggregate was used to derive explicit formulae for calculation of averaging elastic constants. He showed that only two Legendre coefficients of the ODF expansion affect the seismic anisotropy of shales with vertical transversely isotropic (VTI) symmetry. By varying the values of texture coefficients *Sayers* [1994] demonstrated that shales might develop a strong anelliptic anisotropy the degree of which is a function of a single texture parameter, namely, W_{400}. More recently, *Sayers* [2005] compared his ODF model as adapted using a values for an effective clay to another that assumed the anisotropy was controlled by variations in pore compliances between aligned muscovite grains. The elastic values of the effective clay domains were estimated from *Jones and Wang*'s [1981] measurements (Table 2). *Johansen et al.*'s [2004] analysis inserted the anisotropic clay-water layered composites of *Hornby et al.* [1994] into Sayer's Voigt-bound expressions in order to explore the range of anisotropy that might be produced in shales. Instead of employing specific measurements of the ODF $f(g)$, they assumed that it could be more simply described by Gaussian, Fisher, or Bingham statistical distributions; their Gaussian assumption further supported by ODF observations such as those given by *Sintubin et al.* [1995] is employed here also (e.g., Figure 3a).

4.2. Metamorphic Rocks

[16] There have been numerous laboratory studies of mica containing textured rocks and much of this work has been compiled by *Babuška and Cara* [1991]; but only some of the recent contributions have addressed the anisotropy of such rocks in detail, for example by specifying polarization directions of shear waves. *Godfrey et al.* [2000] carried out measurements on a variety of schists to determine their elasticity up to orthorhombic symmetry. *Takanashi et al.* [2001] made measurements on a biotite gneiss and a biotite schist. Although biotite composed no more than 40% of either of these rocks, the anisotropy was found to be primarily due to its texture.

[17] There have been some efforts in modeling the anisotropy of such rocks. *Nishizawa and Yoshino* [2001] calculated the effects of crystal shape on the anisotropy expected for biotite and muscovite aggregates using the differential effective medium theory. They embedded ellipsoidal and anisotropic single crystals in an otherwise homogeneous and isotropic matrix. While they did employ *Alexandrov and Ryzhova*'s [1961] muscovite elastic constants to describe the elasticity of their embedded elliptical crystals, they assumed that the sample and crystal symmetry axes were parallel and as such did not explicitly account for the orientation statistics of the phyllosilicate grains. *Shapiro et al.* [2004] recently attempted to estimate the amount of crustal thinning of the Tibetan plateau on the basis of observed seismic anisotropy on the basis of an ODF produced by simple axial straining of a composite containing biotite and muscovite.

[18] Using an optically obtained ODF for one sample of a natural axially symmetric biotite aggregate, *Mainprice and Humbert* [1994] calculated its elastic phase velocity anisotropy using a variety of models including the geometric mean, the only study that has employed the geometric mean in the context of anisotropic silicate aggregates that is apparent in the literature. The geometric mean velocities, plotted with respect to the inclination of the propagation angle, fell within the more traditional Voigt-Reuss bounds. The values were in good agreement with the Hill average at angles close to the axis of symmetry but diverged significantly at more oblique propagation directions. It must be noted, however, that the geometric mean has been also used to calculate the expected isotropic velocities of rocks on the basis of their mineral modes [*Ji et al.*, 2003].

[19] However, *Takanashi et al.*'s [2001] study is the only complete experimental test in the literature in which the velocities observed in the laboratory have been directly compared to those predicted from the material's mica ODF obtained using X-ray goniometry. Their Voigt bound estimates were in good qualitative agreement with the measurements particularly with respect to the expected symmetry of the material.

5. Texture-Based Modeling and the Geometric Mean

[20] In this section, the theoretical background of the geometric mean modeling employed here is described. As noted above, there are only a limited number of studies in

which the mineralogic texture, as represented by an ODF; has been employed to model the elasticity of an phyllosilicate aggregate.

[21] In our work, modeling of the intrinsic anisotropy is based on the ODF averaging technique [*Viglin*, 1960; *Bunge*, 1982; *Roe*, 1965] in combination with the concept of the ''Geometric mean'' [*Aleksandrov and Aizenberg*, 1966; *Morawiec*, 1989; *Matthies and Humbert*, 1993]. The geometric mean averaging (GMA) technique aims to provide the elasticity of a pore free aggregate. The results obtained here could later be modified using other concepts to include the effects of cracks or other mineral phases. In order to carry out ODF averaging, one needs knowledge of the volumetric fraction of the constituent mineral phases, their elasticity, and the statistics of the textural orientation distributions.

5.1. Classic Voigt-Reuss Averages

[22] Prediction of the elasticity of polycrystalline aggregates is a classic problem in solid mechanics and rock physics with the roots of the investigation coming from early in the last century [e.g., *Voigt*, 1928; *Reuss*, 1929; *Hill*, 1952; *Kröner*, 1958; *Kumazawa*, 1969; *Morris*, 1970; *Thomsen*, 1972; *Watt et al.*, 1976; *Ono*, 1992]. In geophysics, the so-called bounding estimates are well established [*Watt et al.*, 1976]. The simplest, most universal, and widely applied calculations employ the *Voigt* [1928] upper bound that assumes uniform strain and the *Reuss* [1929] lower bound that assumes uniform stress within the isotropic aggregate. The bounds are widely separated for aggregates composed of highly anisotropic crystals [e.g., *Mainprice and Humbert*, 1994]. The degree of texturing of the crystals within the aggregate further influences the separation. Effective medium schemes, such as the already mentioned self-consistent approximation (SCA) method [e.g., *Kröner*, 1978], are frequently applied in the hopes of providing a more constrained solution within the Voigt-Reuss (VR) bounds. However, despite the fact that the SCA solution is unique and converges within the VR bounds, the initial effective medium developments usually require a perfectly disordered aggregate and an absence of correlation between grains shapes and orientations, conditions that may not always hold for the case of a polycrystalline aggregate [*Ono*, 1992]. *Hill* [1952] suggested that the simple arithmetic mean value of the two VR bounds of an isotropic polycrystalline aggregate might be most representative of experimental results [e.g., *Chung and Buessem*, 1967]. The Hill approximation, however, has no solid physical foundation and is applied as a rather simple intuitive solution.

[23] With regard to implementation, integration of the single crystal elastic constants appropriately rotated and weighted by the ODF over all values of g yields elastic constants in the Voigt approximation of uniform strain throughout the aggregate:

$$\overline{C}^{V}_{ijkl} = \int C_{ijkl} f(g) dg \tag{1}$$

where the ODF $f(g)$ is normalized to satisfy

$$\int f(g) dg \equiv 1 \text{ where } dg = \frac{1}{8\pi} \sin\Phi d\Phi d\varphi_1 d\varphi_2 \tag{2}$$

In the discrete orientation space necessary for implementation on a computer, equation (1) can be rewritten in the form

$$\overline{C}^{V}_{ijkl} = \sum_{n=1}^{N} C_{ijkl} f(g_n) \Delta g_n \text{ with } \sum_{n=1}^{N} f(g_n) \Delta g_n \equiv 1 \tag{3}$$

where g_n represents the discretized Euler angle space and Δg_n the corresponding increments.

[24] Equation (3) explicitly defines the elastic constants of polycrystalline aggregate according to the arithmetic mean of the Voigt approximation. The Reuss approximation of constant stress throughout the textured aggregate can be implemented through the procedure similar to equation (1) if the elastic compliances S_{ijkl} are instead used:

$$\overline{C}^{R}_{ijkl} = \left[\int S_{ijkl} f(g) dg \right]^{-1} \tag{4}$$

Note that the averaging procedure in equation (4) yields elastic compliances $\overline{S}^{R}_{ijkl}$ that should be inverted into the elastic stiffnesses $\overline{C}^{R}_{ijkl}$. It is particularly important to note that averaging in either the stiffness or the compliance domains (equations (1) and (4), respectively) yields different solutions [see *Musgrave*, 1970] with $\overline{C}^{R}_{ijkl} \leq \overline{C}_{ijkl} \leq \overline{C}^{V}_{ijkl}$ although the results below show this not to be general in such anisotropic materials. These limits are commonly referred to as the Voigt-Reuss (VR) bounds.

[25] The VR bounds were originally developed for an isotropic medium and generally accepted as the limits to the possible elastic constants to the polycrystalline aggregate [*Hill*, 1952] with the true solution expected at an intermediate value. In the case of the random orientation distribution (i.e., equal probability in all directions) of the constituent anisotropic minerals, the resulting medium is elastically isotropic. Perfectly aligned constituent minerals, on the other hand, create a medium with properties the same as the single anisotropic crystal.

[26] The separation of the VR bounds at this isotropic limit depends solely on the range of values of the elastic constants of the constituent mineral. For strongly anisotropic single crystals as in the present case of muscovite the isotropic Voigt and Reuss bounds of some of the elastic constants differ substantially. For example, values of isotropic muscovite aggregate $C_{11} = C_{22} = C_{33} = \lambda + 2\mu$ (where λ and μ are Lamé parameters) in Figure 4 in the Voigt approximation is 160% of those calculated with the Reuss approximation. Therefore the search for elastic properties of highly anisotropic solids must be modified to overcome these uncertainties.

5.2. Geometric Mean Average

[27] *Aleksandrov and Aizenberg* [1966] first suggested that the invertibility between the elastic stiffnesses and the elastic compliances ($[\int S_{ijkl} f(g) dg]^{-1} = \int C_{ijkl} f(g) dg$), a physical requirement for a real elastic material, be a basis for the search for elastic constants. It is useful to look at the simpler forms for an isotropic system. *Ji et al.* [2004] recently gives a parallel discussion in the context of polymineralic but isotropic aggregates in which the Voigt, Reuss, and geometric means appear as special cases of weighted means. The results for this limiting case are more

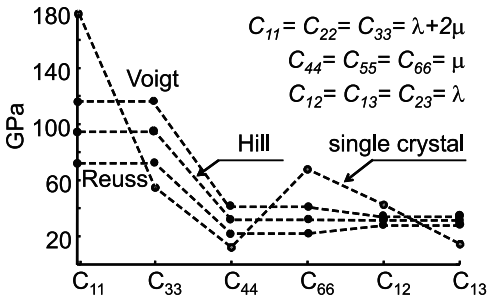

Figure 4. Elastic constants of the muscovite single crystal [after *Alexandrov and Ryzhova*, 1961] (see second row of Table 2) and an isotropic polycrystalline aggregate composed of muscovite crystals in the Voigt, the Reuss, and the Hill approximations. Elastic constants $C_{11} = C_{33}$ in the Voigt approximation are 160% of those in the Reuss approximation.

directly seen as the orientation distributions are uniform in all directions and reduce to simpler modal volume fractions V_i with

$$\overline{R} = \exp\left[\sum_{j=1}^{N} V_j \ln(R_j)\right] = \prod_j R_j^{V_{ij}} \tag{5}$$

where R here applies to the isotropic Young's, bulk, or shear moduli *E, K*, and ν, respectively. The resulting GMA moduli lie not only within the VR bounds but also within the narrower *Hashin and Shtrikman* [1963] bounds.

[28] More recently, *Morawiec* [1989] and *Matthies and Humbert* [1993] further extended the GMA method to estimate the elastic constants of textured polycrystalline aggregates which are expected to be anisotropic. They calculated the Young's modulus of a hypothetical *Zn* sample and found good agreement between the GMA and the self-consistent approaches. *Mainprice and Humbert* [1994] first applied the GMA technique to less symmetric silicates as noted earlier. Their results showed that the GMA is close to the Hill solution for both compressional (V_p) and shear (V_s) values except at large angles relative to the axis of symmetry. These authors concluded "the geometric mean is the best estimate of the seismic properties of the simple averaging methods" *Mainprice and Humbert* [1994, p. 590]; however, further development of the GMA in the context of anisotropic silicate aggregates is not reported in the literature.

[29] There are several major factors that influence the intrinsic anisotropy of a solid rock matrix including the elasticity of the constituent minerals, their volumetric fraction and their texture (ODF) within the aggregate. Following *Bunge* [1982], the averaged elastic constants $\overline{C}_{ijkl}$ of a nonporous textured monomineralic polycrystalline aggregate depend on the elastic constants C_{ijkl} of the mineral, the mineral's symmetry, and the statistics of the orientations of the mineral relative to the aggregates frame of reference usually via the ODF [*Musgrave*, 1970]. Details are provided in Appendix A, but, briefly, in order to understand the solution, it is conceptually useful to consider the contribution of a single crystal with a given orientation g′. In order to carry out the average for the rock, one must first calculate the form of this crystal's elastic constants $C'_{ijkl.}$ rotated into the aggregate coordinate frame. This process would then be repeated for each crystal with different orientations in the aggregate; the resulting rotated values may then be averaged after being appropriately weighted by each crystal's volumetric proportion. Of course, in practice, the weighting is done statistically using the ODF. The details of this process are summarized in Appendix A, but they do rely on eigenvalue decomposition of the single crystal elastic constants and expansion of the ODF $f(g)$ by symmetrical generalized spherical harmonics, the latter specially constructed for the problem of averaging a TI crystal into a TI aggregate. The spherical harmonic approach is advantageous as it simultaneously includes the elements of both the crystal and aggregate symmetries and of the texture through the ODF.

6. Results

[30] It has been mentioned above that the elasticity of an aggregate matrix varies with the texture, and as such, one might expect the elasticity to lie between two extreme limiting cases of a perfectly aligned aggregate that is indistinguishable from the single crystal and an isotropic aggregate with completely random crystal orientations. The resulting averaged elastic constants are, by definition, dependent on the alignment of the crystalline x_i (i = 1,2,3) and rock coordinate systems X_j (j = 1,2,3). For the case of fully aligned crystallite equations (A7) and (A8) describe this dependence and values of the textural coefficients B_2^{11} and B_4^{11} can be directly incorporated into the averaging procedure.

[31] Investigation of the effect of the different averaging procedures on the intrinsic anisotropy as a function of axially symmetric textural strength would provide more insight. If the [001] crystallographic axis of the constituent hexagonal mineral in the TI aggregate is aligned with X_3, then the aggregate elasticity depends only on the elasticity of the single crystal. A perfectly aligned aggregate has the elastic properties of a single crystal; all three coefficients of the ODF expansion (namely, B_0^{11}, B_2^{11} and B_4^{11}) are nonzero and contribute to the averaging. As noted above, in real shales and schists, the [001] textural distribution peak is distributed around the X_3 foliation normal. This distribution can be approximated by the normal (Gaussian) distribution function [e.g., *Johansen et al.*, 2004] characterized by the standard deviation σ of Φ with mean value M:

$$f(\Phi) = k(\sigma)\exp\left[-\frac{1}{2}\left(\frac{\Phi - M}{\sigma}\right)^2\right] \tag{6}$$

where $k(\sigma)$ is an appropriate scaling factor.

[32] The lower limiting value $\sigma = 0$ (i.e., no variation in the orientations of all the crystals in the aggregate) corresponds to a single crystal. Increasing disorder in the orientations results corresponds to larger values of σ and a broader Gaussian curve (Figure 5) Eventually, distribution of the [001] axis can be treated as quasi uniform within the aggregate with no specific preferential orientation and, therefore, resemble a random distribution of the crystals.

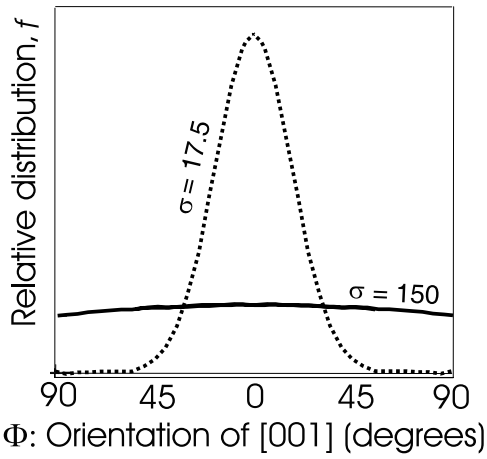

Figure 5. Broadening of the Gaussian function describing $f(\Phi)$ with increasing values of the disorder as measured by the standard deviation σ of the orientations.

For all practical purposes this is achieved for $\sigma = 150°$. For the random orientation distribution the only nonzero texture coefficient is B_0^{11} [*Bunge*, 1982]. By definition $B_0^{11} \equiv 1$ and the averaging of this single coefficient over the elastic stiffnesses yields the well-known isotropic solution in the Voigt approximation [e.g., *Simmons and Wang*, 1971]. The identical averaging procedure over the elastic compliances yields the isotropic Reuss elastic compliances. Therefore $B_0^{11} \equiv 1$ can generally be treated as an isotropic part of arbitrary texture that is described by the coefficients $B_l^{\mu\nu}$.

[33] The elastic stiffnesses of the aggregate with different degrees of orientation disorder are shown in Figure 6. The value of the elastic constants at $\sigma = 0$ is that of the single crystal limit (marked by XTL). The value for $\sigma = 150°$ is for an isotropic aggregate (marked by ISO). The Voigt, Reuss, Hill and geometric mean averaging results are all shown for comparison. The Geometric mean averages are generally close to, but can lie either above or below, the Hill value for constants along the stiffness matrix's diagonal. The behavior of the off-diagonal constants is more complex. The GMA C_{12} deviates from the Hill and approaches the Voigt value as the material becomes more disordered. The GMA C_{13} exceeds the values of the other averages at all measures of disorder and does not fall within the V-R bounds. The GMA elastic constants have values close to either the upper or the lower bound depending on the aggregate's texture. To further complicate matters, proximity of the GMA solution to either the Voigt, the Reuss or the Hill averages differs from constant to constant in anisotropic solid.

[34] The importance of this result is that the rigid constrains of the Hill approximation with respect to the VR bounds might not be very suitable for accommodating elastic behavior of anisotropic solids. Values of the elastic constants (namely, C_{12} and C_{13}) for particular range of textural strength do not necessarily lie within the VR bounds. Notice also that the Voigt and Reuss values even cross for a certain range of σ for C_{13} coefficient (Figure 6) and therefore for this case cannot be treated as bounds per se.

[35] The resulting *qP*, *qSH*, and *qSV* elastic wave phase-slowness surfaces from isotropic to single crystal (Figure 7) are calculated using the texturally dependent elastic stiffnesses (Figure 6) in Christoffel's equation [e.g., *Musgrave*, 1970]. These curves display much of the general behavior observed in anisotropic rocks, particularly shales. At $\sigma = 150$ approaching randomly orientations, the slowness curves are circular as is expected for an isotropic aggregate. For smaller values of σ indicative of preferential orientations, both the *P* and *SV* slownesses are anelliptic while those of *SH* mode are always elliptical. The *P* and *SH* vertical (X_3) velocities are always less than those for the corresponding isotropic aggregate.

7. Discussion

7.1. Anisotropic Parameter Behavior

[36] The elastic properties of the weakly transversely isotropic medium are often characterized by a variety of dimensionless parameters [e.g., *Thomsen*, 1986; *Carrion et al.*, 1992; *Tsvankin and Thomsen*, 1994; *Alkhalifah and Tsvankin*, 1995]. Parameterizations are designed to simplify the description of anisotropic elastic behavior and reduce the number of initially unknown coefficients. It should, however, be stressed that parameterization of anisotropic medium should not aim to replace more fundamental elastic constants but rather to simplify description of the elastic behavior.

[37] For a transversely isotropic medium, *Thomsen* [1986] developed approximations to the full elastic equations and introduced three anisotropy parameters $\varepsilon = (C_{11} - C_{33})/2C_{33}$, $\delta = [(C_{13} + C_{44})^2 - (C_{33} - C_{44})^2]/2C_{33}(C_{33} - C_{44})$ and $\gamma = (C_{66} - C_{44})/2C_{44}$ the influence of the variations of which are illustrated for an example in Figure 8. It is useful to briefly review the effects of these parameters. ε and δ can be considered as measures of the anisotropy of the longitudinal and the *SV* polarization shear waves. The *SH* velocities depend only on γ and delineate an ellipse. *Thomsen* [1986] focused on the effects of anisotropy on near-offset reflection seismic move out curves and interpreted his δ in this light with a rather vague physical meaning reflecting the *P* wave phase velocity dependence on the direction in the vicinity of the vertical incidence angle. Examination of his equations (16) in the current context suggests that δ can also be considered as one measure of the anellipticity (i.e., the deviation from an elliptical reference) of the *P* wave curve. Other workers have used similar measures of annelipticity [*Gassmann*, 1964; *Carrion et al.*, 1992; *Sayers*, 1995]. The value of δ, or more precisely its value relative to ε, controls whether the curve (Figure 8) is concave ($\delta < \varepsilon$), elliptical ($\delta = \varepsilon$), or convex ($\delta > \varepsilon$). The simple difference $\varepsilon - \delta$ relates more directly to the anellipticity of the *SV* polarization shear giving curves that are concave ($\delta > \varepsilon$), circular ($\delta = \varepsilon$), or convex ($\delta < \varepsilon$) relative to the *SH* ellipse. Again, variations of $\eta = \varepsilon - \delta$ have been employed in other contributions [*Tsvankin and Thomsen*, 1994; *Alkhalifah and Tsvankin*, 1995] but the simple difference is retained in the analysis below in order to minimize the uncertainties of the experimental measurements. It must again be reiterated that for the full elastic equations the *P* and *SV* curves do not, aside from the limit of isotropy, follow ellipses or circles as do the illustrations of Figure 8 calculated using *Thomsen*'s [1986] approximations.

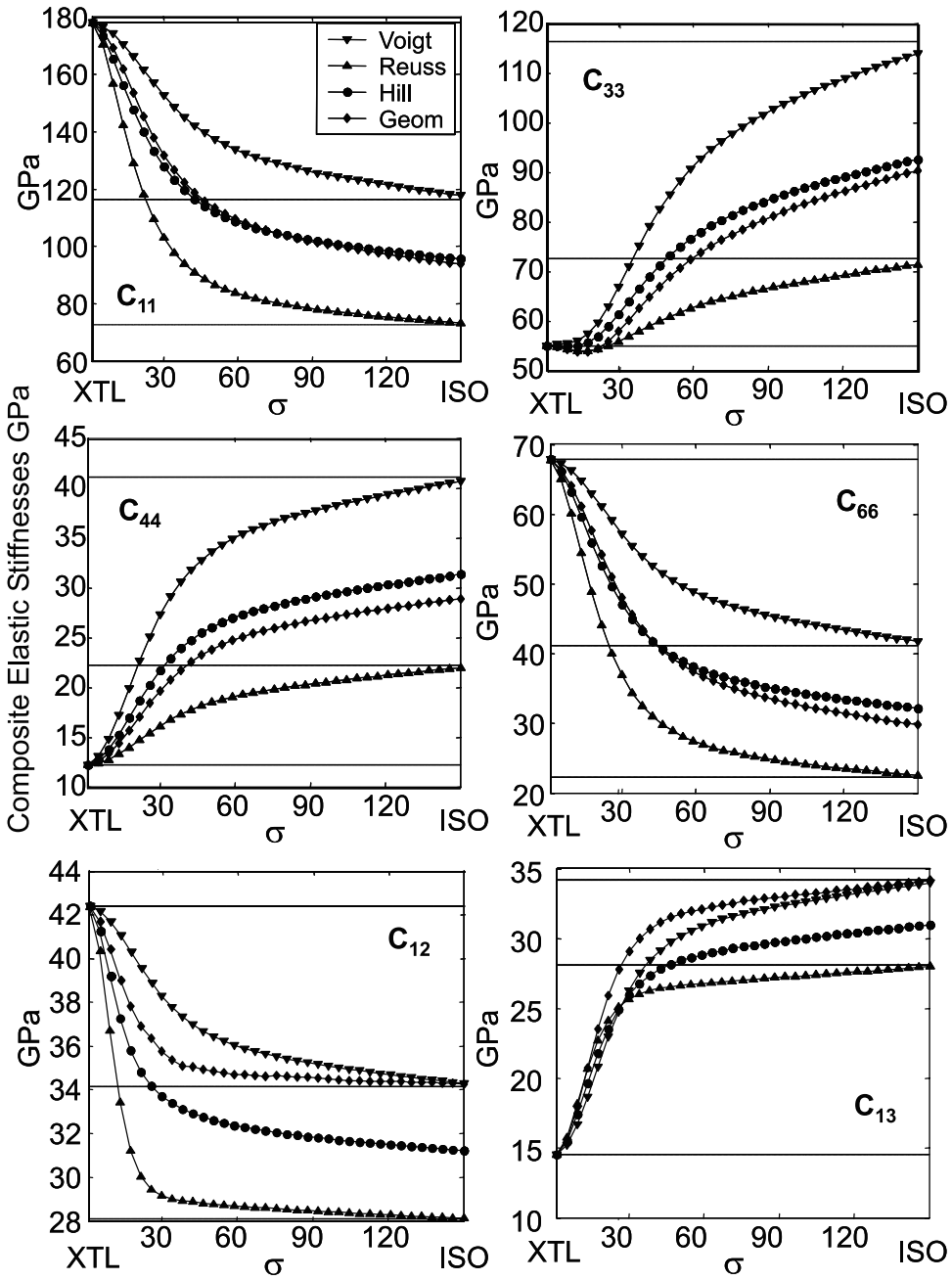

Figure 6. Elastic constants of the TI muscovite matrix as a function of textural strength, defined by the standard deviation of the Gaussian distribution σ of clay platelet normals from the bedding plane normal (see text for details). The left end of the ordinate axis for each plot represents values of fully aligned polycrystalline aggregate with the properties of a single crystal (XTL). The right end represents quasi-isotropic aggregate (ISO). Constant dashed lines show values of the elastic constants of the single crystal and the isotropic Voigt and Reuss solutions.

[38] For completeness, these parameters are calculated from the elastic constants of Figure 6 and plotted as a function of the strength of texture over the entire range in Figure 9; again it must be noted that these parameterizations may not be appropriate for the higher anisotropies encountered for the strongly textured materials (i.e., small σ). Both, ε and γ behave similarly and decay from the maximum single crystal value to zero for the isotropic aggregate. δ has a more complex behavior being negative for the single crystal, but increasing to at least the same positive value before eventually decaying toward zero for the quasi isotropic aggregate. η monotonically increases toward zero as the degree of disorder increases, $\eta \leq 0$ also for all textures meaning that the *P* and *SV* curves are anelliptically concave and convex, respectively. It is interesting to note that for a certain range of textural strengths, δ is sensitive to the averaging method with the Voigt values several times those for the Reuss.

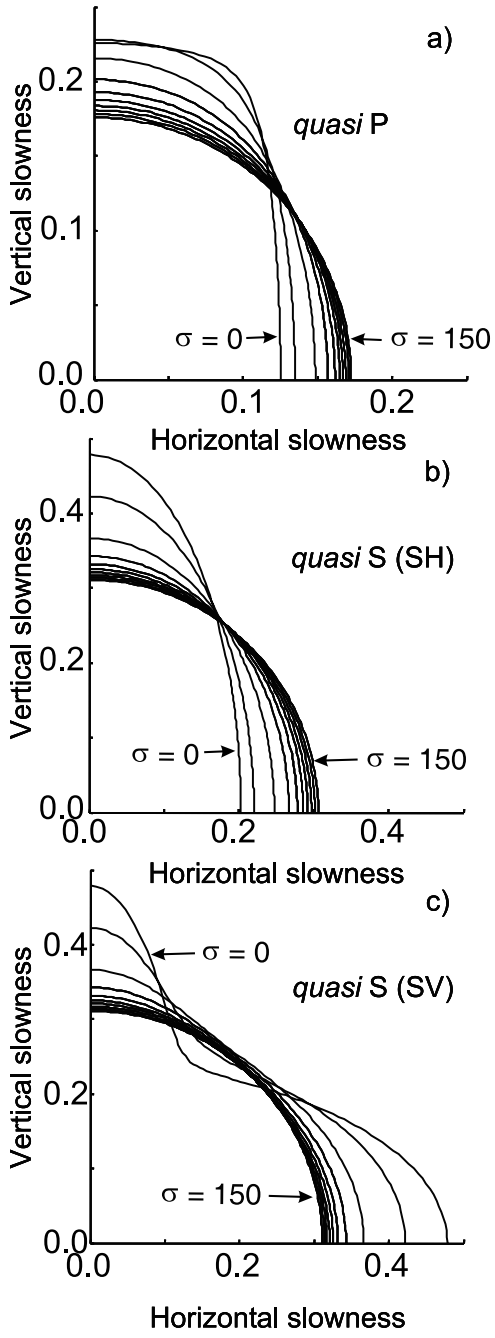

Figure 7. Slowness surfaces for *qP* and *qS* (*SH* and *SV*) waves for intrinsically anisotropic shale of TI symmetry calculated from the elastic constants obtained by the GMA procedure in Figure 6 with a density of 2790 kg/m^3. Slowness surfaces vary from highly anisotropic for a single crystal to almost circular for quasi-isotropic aggregate. Surfaces are plotted in increments of $\sigma = 10°$.

[39] The resulting curves of η for the Voigt, Reuss, Hill, and GMA averages all yield nearly the same value of anellipticity as shown on Figure 9. Despite the fact that the various averaging procedures give different absolute values of elastic constants, the overall behavior of the elastic waves (especially anellipticity) predicted by these approximations is similar.

7.2. Comparison of Anisotropy Parameters to Laboratory Measurements

[40] The crossplotting of the theoretical anisotropic parameters from Figure 9 against each other in Figure 10 provides additional insight into the anisotropic behavior of the hypothetical muscovite aggregate and serve as a measure against which the laboratory observations may be compared. In Figure 10, the geometric mean, the Voigt, and the Reuss solutions are separately plotted as solid, dashed, and dash-dotted lines, respectively. All three averages diverge from the isotropic condition ($\varepsilon = \delta = \gamma = 0$) as the muscovite orientations become more ordered. γ increases at nearly the same rate and almost linearly with ε. The behavior of δ is more complex, in the ε versus δ and γ versus δ curves the geometric mean and the Voigt solutions are close to one another and significantly diverge from the Reuss predictions. The curve for the geometric mean average, however, does show that δ increases with both ε and γ at close to half their rate as might intuitively be expected for an increasingly anisotropic material. Curves for η are also included for completeness. η increases with both ε and γ as might be anticipated, but has a more complex behavior in relation to δ.

[41] There are a number of laboratory ultrasonic velocity studies on shales and schists in which all or some of the elastic stiffnesses have been obtained. The bulk of the work has focused on shales [*Jones and Wang*, 1981; *Johnston and Christensen*, 1995; *Vernik and Liu*, 1997; *Wang*, 2002] but with some recent but less numerous measurements on metamorphic schists [*Takanashi et al.*, 2001; *Godfrey et al.*, 2002; *Cholach et al.*, 2005] The results of these observations are also included in the crossplots of the

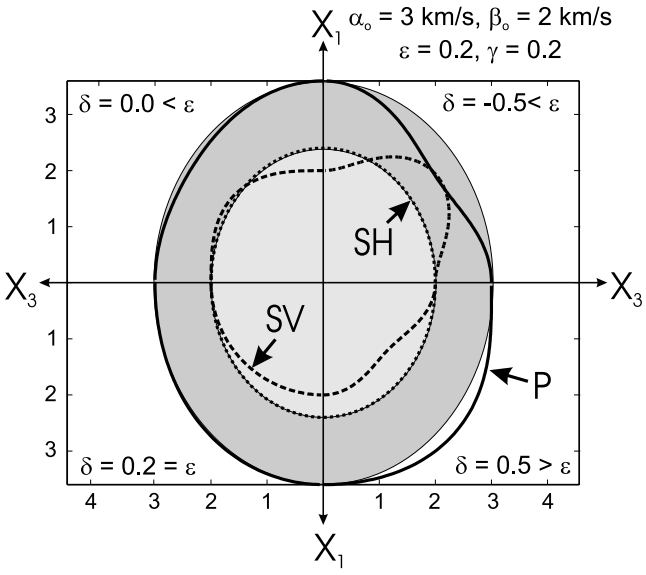

Figure 8. Illustration of the influence of ε, γ, and δ on the phase velocities of a weakly transversely isotropic medium. The cases of $\delta < \varepsilon$, $\delta = 0 < \varepsilon$, $\delta = \varepsilon$ (elliptical condition), and $\delta > \varepsilon$ correspond each to a quadrant of the figure. The reference ellipses are filled with light and dark grey corresponding to the longitudinal and *SH* polarization shear waves, respectively.

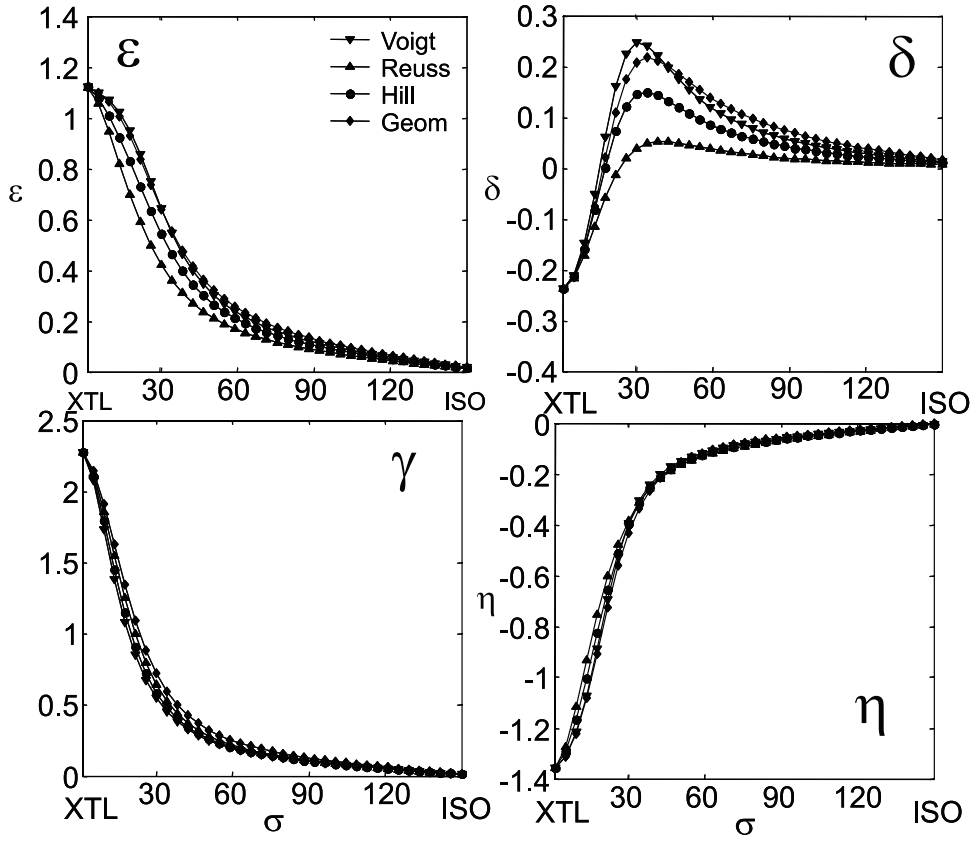

Figure 9. Anisotropic parameters ε, γ, δ and $\eta = \delta - \varepsilon$ for TI medium as a function of textural strength (same as Figure 6). All parameters approach zero for an isotropic aggregate.

anisotropic parameters in Figure 10 with shales and metamorphic schists represented as open circles and squares, respectively. The focus of most of these studies were primarily on the velocity anisotropy itself and only a few provide detailed petrographic characterizations that included mineralogy and, as noted earlier, only one has explicitly provided measures of the corresponding phyllite ODF [*Takanashi et al.*, 2001]. Other high-quality anisotropy determinations, notably that of *Vernik and Nur* [1992], were excluded as they considered anisotropic materials containing substantial fractions of kerogen.

[42] Experimental uncertainties are rarely provided in such studies. Consequently, one recent measurement of anisotropy on a layered kerogen rich but clay absent rock ("Colorado Oil Shale") by *Mah* [2005] has been included in Figure 10 only to illustrate the levels of experimental uncertainty that are encountered. Mah's ε and γ uncertainties are small and are substantially less than the size suggested by the symbol in Figure 10a. Determination of δ, however, requires that it be calculated from a number of the elastic constants and when the errors are propagated δ becomes highly uncertain, *Mah*'s [2005] measurements suggest that the uncertainty in δ is approximately 0.065, a value on the order of the magnitude of δ itself.

[43] Admittedly, this crossplotting was done naively in that none of the rocks are composed only of muscovite. Consequently, if it is assumed that the geometric mean average does provide the best measure of the expected anisotropy of the muscovite aggregate, then it is the deviations of the experimental results from these theoretical predictions that are of most interest.

[44] The large scatter of the experimental results makes definitive conclusions difficult particularly when the large uncertainties in δ are considered. However, some trends do appear. The experimental γ correlates positively with ε (Figure 10a) but the bulk of the experimental measurements fall below the aggregate trend lines particularly for more weakly anisotropic rocks. This may suggest that the *qSV* and *qSH* anisotropy in these rocks is weaker than that for *qP*. One should note, however, that for the metamorphic rocks, the *qS* anisotropy exceeds that for the *qP* consistent with *Okaya and Christensen*'s [2002] observations. In contrast, δ does not appear to correlate with ε. The values of δ in the range $\varepsilon < 0.25$ center near zero and even when the large potential uncertainty in δ is considered, the values lie below the trend lines, suggesting that the *qP* and *qSV* velocities will be more concave and convex, respectively, than their corresponding reference ellipses. The correlation between δ and γ is even weaker.

[45] The modeling presented here is based on several assumptions that include the phyllite's mineralogical composition, the elasticity of the constituent minerals and their orientations. These assumptions may not hold in more realistic rocks and the consequences of these approximations leading to the divergence of the theoretical predictions and the laboratory ultrasonic observations need to be discussed.

[46] The first and most obvious, already mentioned, is that the real rocks are not pure muscovite aggregates. These

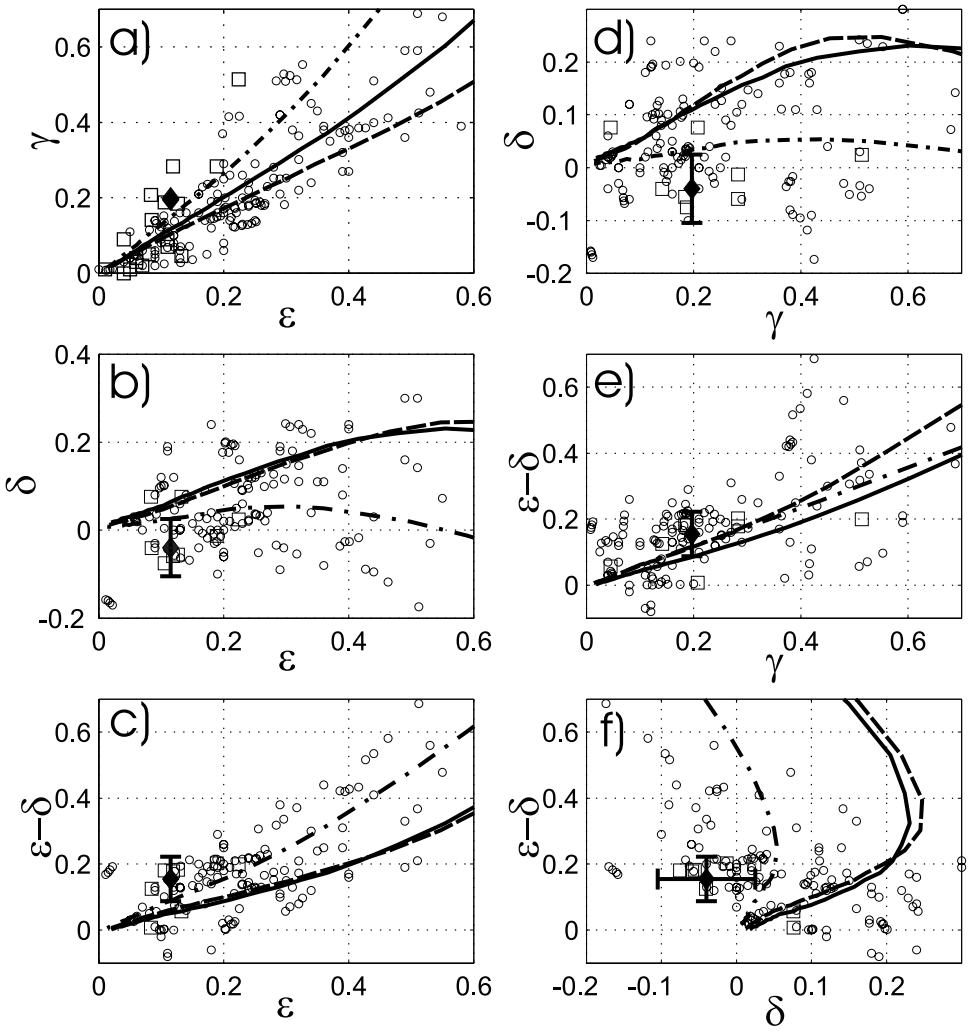

Figure 10. Crossplots of the anisotropic parameters: (a) ε versus γ, (b) ε versus δ, (c) ε versus $\varepsilon - \delta$, (d) γ versus δ, (e) γ versus $\varepsilon - \delta$, and (f) δ versus $\varepsilon - \delta$. Lines represent theoretical averages for the muscovite aggregate: solid line, geometric mean; dashed line, Voigt average; dash-dotted line, Reuss average. Each of these lines begins at the origin (for $\sigma = 150°$) and ends at $\sigma = 0°$. Symbols represent values taken from the literature: open circles, shales [*Jones and Wang*, 1981; *Johnston and Christensen*, 1995; *Vernik and Liu*, 1997; *Wang*, 2002]; open squares, *Takanashi et al.* [2001], *Godfrey et al.* [2002], and *Cholach et al.* [2005]. Solid diamonds with error bars are from the laboratory measurements of *Mah* [2005] and are shown only to indicate the high level of uncertainty associated with δ.

rocks include other mineral phases and in the case of many shales, organic compounds, that both dilute and disrupt the orientations of the phyllite minerals. Other inhomgeneities include cracks and pores, layering at many scales, and fluids.

[47] Second, knowledge of the true elasticity of the constituent minerals, particularly for illite, will be essential for proper modeling of the intrinsic elasticity and, subsequently, determining the seismic velocities. The elastic constants of constituent minerals predefine intrinsic elasticity of the highly textured aggregates and influence the absolute values of the elastic constants in quasi-isotropic aggregates with randomly oriented minerals. The presence of phases such as quartz, feldspars, and carbonates, the modes of which often do not correlate with anisotropy, also affect the overall elasticity and reduce the anisotropy. The reduction is dependent on the volumetric presence of each of these phases. A substantial volumetric presence of randomly oriented and spatially distributed silt particles in shales also interferes with the alignment of the clay minerals [e.g., *Hornby et al.*, 1994]. Further, the elastic properties of more complex smectites that can form a substantial proportion of shales are not at all understood.

[48] Detailed examination of the compilation on phyllite mineral elasticity in Table 2 may reveal some deficiencies in the use of the current muscovite stiffnesses in the modeling. To briefly summarize, the elastic constants obtained from measurements on single crystals of mica exceed substantially those estimated from measurements on clay composites or on clay containing rocks. Various authors [e.g., *Hornby et al.*, 1994; *Johansen et al.*, 2004; *Sayers*, 2005] have attempted to overcome this discrepancy by employing a clay domain in which the "effective" single crystal elasticity is reduced either by cracks or layers of fluid.

[49] This discrepancy, also noticed by *Vanorio et al.* [2003], is not understood and at this point in our understanding only some speculations are available. Some of the differences are likely due to the variations in composition with the values inferred from rocks being influenced by the existence of wetting smectites. One other possible reason arises from the large unbalanced charges that exist on the surfaces of such minerals [e.g., *Israelachvili et al.*, 2004]; the existence of like static negative electric charges on mica and clay surfaces would introduce repulsive forces between the individual crystals that may act to reduce the effective moduli of the mineral.

[50] One final possible reason for the discrepancy between the muscovite aggregate and the laboratory observations in Figure 10 may relate to the assumption that many phyllitic rocks, and particularly shales, will be transversely isotropic. However, phyllite mineral ODFs are not necessarily axially symmetric as indicated by *Oertel* [1983], *O'Brien et al.* [1987], and *Sintubin* [1994b] with varying degrees of orthorhombicity apparent in materials that have undergone some tectonic straining. The peaks of an ODF need not even necessarily be perpendicular to the foliation, *O'Brien et al.* [1987] show a biotite [001] ODF from a mylonite that displays a nearly Gaussian distribution the peak of which, however, is shifted nearly 10° from X_3.

[51] As has been shown the intrinsic elasticity of shales is significantly influenced by texture. The degree of the mineral platelet alignment (i.e., texture strength) varies substantially in shales and depends on several factors such as the state of compaction (i.e., function of depth) and maturation [e.g., *Vernik and Liu*, 1997; *Hornby*, 1998] and diagenetic processes [*Ho et al.*, 1999]. Intrinsic elastic anisotropy may vary from high anisotropy for perfectly aligned clay aggregates to quasi-isotropic for the case of almost randomly distributed clay platelets orientation. A further assumption of no lateral preferences in the orientation of normals of the clay platelets is usually made. Under this assumption the matrix composed of hexagonal crystals has TI statistical symmetry. Knowledge about the hexagonal symmetry of the constituent minerals and the TI symmetry of the matrix allows the number of independent coefficients in the ODF expansion to be reduced. The assumption of no preferred lateral orientation may not hold in the presence of additional textural features such as microfolding caused by the tectonic stresses, which may lower the statistical intrinsic elastic symmetry from TI to orthotropic or lower.

[52] Finally, the overall elasticity of shales (especially in the fluid-rich conditions) depends not only on its intrinsic properties but also on the presence of oriented microcracks [e.g., *Vernik*, 1993], the amount of the fluid-filled porosity [e.g., *Hornby*, 1998] and the in situ distribution of stresses [*Sayers*, 1999], i.e., factors that may significantly influence anisotropy and cannot be ignored. Models that incorporate these factors would, however, benefit by starting from the intrinsically anisotropic matrix.

8. Conclusions

[53] The intrinsic elasticity of a muscovite aggregate has been modeled by the orientation distribution function (ODF) averaging of the elastic constants of muscovite, a mica structurally similar to illite. The generally accepted approximations based on the assumptions of uniform strain and stress within the solid matrix yield, correspondingly, the Voigt and the Reuss averaging solutions. The VR bounds are widely separated which allows significant variation in the values of intrinsic elastic constants of shales. To overcome this limitation, the geometric mean averaging (GMA) method has been incorporated into the ODF averaging procedure. The GMA provides a solution fulfilling the requirement of invertibility between aggregate stiffnesses and compliances. This solution lies predominantly relatively close to the Hill average within the VR bounds for the diagonal elastic constants.

[54] The purpose of implementation of the GMA solution was to examine the effect of the texture strength per se on the elasticity of phyllite matrix, the Voigt and Reuss bounds on the individual elastic stiffnesses progressively diverge as the crystals become more randomly oriented. The GMA results vary with respect to the VR bounds (compare the Hill solution). This implies that neither the Voigt, the Reuss nor the Hill approximation uniquely define the elasticity of highly anisotropic aggregates; the elastic constants of an anisotropic solid obtained by GMA method may lie close to any of these solutions depending on the values of the elastic constants of the constituent minerals and aggregate texture.

[55] Slowness surfaces calculated from the GMA elastic constants show significant anellipticity of *P* wave surface for the highly textured aggregate. In addition, it is clear that axial *P* and *S* wave velocities of a textured muscovite aggregate with VTI symmetry are always slower than that for the isotropic aggregate. Measures of the *P* and *SH* wave anisotropy (ε and γ) are both positive and monotonically decrease as the crystal orientations become more random. The parameter δ, however, reaches a peak for a highly textured aggregate after which it smoothly decreases to zero. Crossplots of the various parameters indicate that the *P* and *SH* wave anisotropies ε and γ increase together at nearly the same rate, δ increases more slowly.

[56] A number of high-quality ultrasonic laboratory measurements of anisotropy on schists and shales are compared to the theoretical crossplots. While there is a large degree of scatter in these experimental results, they indicate that relative to the muscovite aggregate the *S* wave anisotropy decreases more slowly with greater orientation disorder than the *P* wave anisotropy. The observed δ cluster near zero and do not appear to correlate strongly with either ε or γ. One should not expect the laboratory observations on real rocks to be described exactly by the theoretical muscovite aggregate curves, however, as a large number of other factors such as layering, porosity, and fluids influence overall elasticity and anisotropy. The GMA curves developed here for the elastic constants and the velocity surfaces and anisotropic parameterizations that follow should be taken as a reference point upon which more inclusive modeling can be carried out, although carrying out additional GMA calculations using ODFs observed on real rocks or predicted from strain-deformation theories would be useful also. While the crossplotting of anisotropic parameters is useful, the value of the experimental measurements to understanding the source of anisotropy in such rocks would be increased by more intensive material characterizations.

[57] Finally, the modeling here has assumed particular values for the single crystal elastic stiffnesses. Examination

of Table 2, however, shows a large degree of uncertainty as to what the elastic properties of micas and particularly clays actually are. Generally, the single crystal stiffnesses and bulk moduli substantially exceed those measured on aggregates. The reasons for this are not known although they may be related to the role of water and unbalanced charges on the mineral surfaces; and a better understanding of the behavior of these crystals is required.

Appendix A

[58] Knowledge of both the single crystal elastic constants, represented below as the matrix C, and of the mineral's ODF within the aggregate $f(g)$ is first required. Both of these are expanded first prior to the averaging procedure.

A1. Spherical Harmonic Expansion of *f(g)*

[59] In order to obtain this unique solution textural information is incorporated via $f(g)$ (equation (8)). Following *Bunge* [1982], $f(g)$ may be expanded into the series of symmetrical generalized spherical harmonics referred to as a *Viglin* [1960] expansion:

$$f(g) = \sum_{l=0}^{\infty} \sum_{m=-l}^{+l} \sum_{n=-l}^{+l} B_l^{mn} T_l^{mn}(g) \tag{A1}$$

where T_l^{mn} are generalized spherical harmonics (GSH) and the B_l^{mn} are constants, representing the magnitude of the corresponding harmonic in the expansion. The advantage of the Viglin expansion is that the GSH in equation (A1) can be further modified to reflect the specific rock and constituent mineral symmetries via

$$f_4(g) = \sum_{l=0}^{4} \sum_{\mu=1}^{M(l)} \sum_{\nu=1}^{N(l)} B_l^{\mu\nu} \ddot{T}_l^{\mu\nu}(g) \tag{A2}$$

where for the case considered in this paper the $\ddot{T}_l^{\mu\nu}(g)$ are symmetrical generalized spherical harmonics (SGSH) specially constructed to fulfill both the aggregate's transverse isotropy and the single crystal hexagonal symmetry properties. The $B_l^{\mu\nu}$ are coefficients of the SGSH that carry information about the aggregate texture and are described below. $M(l)$ is the number of linearly independent spherical harmonics required for a specific symmetry. Note that $f_4(g)$ represents truncation (to the degree $l = 4$) of the infinite expansion series of $f(g)$ (equation (A1)). The maximum degree of the ODF expansion in equation (A2) corresponds to the order of the tensor that describes the particular physical properties of the rock. The elastic properties of the solid material can be fully described by the fourth-order elasticity tensor C_{ijkl} (or S_{ijkl}); consequently the coefficients of the ODF expansion of $l = 4$ are sufficient for the averaging procedure [*Backus*, 1970].

[60] It must be noted that *Sayers'* [1994] development is based on the *Roe* [1965] formalism, which differs in how $f(g)$ is normalized (equation (2)). In the Roe formalism, the coefficients of the Viglin expansion must be adjusted to accommodate the rock and the constituent crystal symmetries. In the *Bunge* [1982] formalism adopted here the generalized spherical harmonics intrinsically reflect both the rock and constituent crystal symmetries [*Ferrari and Johnson*, 1988]. For the transversely isotropic aggregate only five coefficients $B_l^{\mu\nu}$ of the expansion (namely, B_2^{11}, B_2^{21}, B_4^{11}, B_4^{21}, B_4^{31}) are nontrivial. Furthermore, when the infinite symmetry (i.e., rotational) axis of the TI medium is aligned with the X_3 axis of the right handed $X_1X_2X_3$ aggregate coordinate system, the coefficients B_2^{21}, B_4^{21} and B_4^{31} vanish (reflecting hexagonal crystal symmetry: $B_l^{\mu\nu} = 0$, if $\mu \neq 1$, [*Bunge et al.*, 1981] and only two coefficients B_2^{11} and B_4^{11} contribute to the elasticity of the aggregate (compare with W_{200} and W_{400} in Sayers development). The additional coefficient $B_0^{11} \equiv 1$ carries an isotropic component in the expansion and must be taken into account.

[61] Following *Bunge* [1982], the coefficients of the expansion can be written (taking into account orthonormal properties of the SGSH)

$$B_l^{\mu\nu} = (2l+1) \int f(g) \ddot{T}_l^{*\mu\nu}(g) dg \tag{A3}$$

[62] In the case of hexagonal-TI symmetries all the SGSH in expansion are real (m and n in equation (A1)) are even) and the complex conjugate symbol (asterisk) may be omitted. For the aggregate that consist of a single crystal with specific orientation taking into account normalization (2) equation (A3) can be simplified to

$$B_l^{\mu\nu} = (2l+1) \ddot{T}_l^{\mu\nu}(g_0) \tag{A4}$$

where g_0 is an orientation of the aligned single crystal. Calculation of the expansion coefficients $C_l^{\mu\nu}$ can further be simplified if one takes into account that $\ddot{T}_l^{\mu\nu} = P_l^{\mu\nu}$ for $\mu = 1$ and $\nu = 1$, where $P_l^{\mu\nu}(\cos\Phi)$ are the generalized associated Legendre functions (GALF). It should be noted that the GALF are functions of only one Euler angle Φ and the ODF of hexagonal-TI symmetry is independent of the φ_1 and φ_2. *Bunge* [1982] showed that the GALF can be represented by a Fourier series:

$$P_l^{\mu\nu}(\Phi) = \sum_{s=-l}^{+l} a_l^{\mu\nu s} e^{is\Phi} \tag{A5}$$

where $a_l^{\mu\nu s}$ are Fourier expansion coefficients. For $\mu + \nu$ even equation (A5) can be rewritten

$$P_l^{\mu\nu}(\Phi) = \sum_{s=0}^{+l} a_l'^{\mu\nu s} \cos(s\Phi) \tag{A6}$$

coefficients $a_l'^{\mu\nu s}$ were tabulated by *Bunge* [1982] and the coefficients of the SGSH for the ODF consistent of single crystal can finally be written in a simple form of the combination of cosine functions:

$$B_2^{11} = 5(0.25 + 0.75\cos(2\Phi)) \tag{A7}$$

$$B_4^{11} = 9(0.140625 + 0.3125\cos(2\Phi) + 0.546875\cos(4\Phi)) \tag{A8}$$

A2. Implementation of the Geometric Mean

[63] Following *Matthies and Humbert* [1993], C, the matrix representing the single crystal's elastic constants is

decomposed into Λ^0, a diagonal matrix of eigenvalues μ^0, and its corresponding the orthogonal matrix of eigenvectors W:

$$C = W\Lambda^0 W^T \tag{A9}$$

For the geometric mean average, the natural logarithms of the eigenvalues are calculated to form the diagonal matrix $\overline{\Lambda}^0$, which is then applied to determine the aggregate's elastic constant matrix $\langle C\rangle$ from the ODF averaging:

$$\langle C\rangle = \int W\overline{\Lambda}^0 W^T f(g)dg \tag{A10}$$

$\langle C\rangle$ may then itself be decomposed into a new set of eigenvalues ν_k that make up a diagonal matrix Λ with orthogonal matrix U

$$\langle C\rangle = U\Lambda U^T \tag{A11}$$

To bring the solution back to a physically meaningful form, $\overline{\Lambda}$ is then the diagonal matrix composed of the exponents of the eigenvalues ν_k obtained from the eigenvalue decomposition of the matrix $\langle C\rangle$, which yields, in matrix form, the desired geometric mean average elastic constants $\langle\overline{C}\rangle$ for the aggregate:

$$\langle\overline{C}\rangle = U\overline{\Lambda}U^T \tag{A12}$$

In reduced Voigt notation and with Einstein summation conventions [see *Nye*, 1990] this final result is explicitly

$$\langle\overline{C}_{ij}\rangle = U_{ik}\exp(\nu_k)U_{kj} \tag{A13}$$

where $\langle\overline{C}_{ij}\rangle$ are the geometric mean averaged elastic constants of the polycrystalline aggregate.

[64] Equations (A9)–(A13) implement *Aleksandrov and Aizenberg*'s [1966] concept for an anisotropic solid by averaging the modified eigenvalue functions of the stiffnesses or the compliances rather then directly averaging stiffnesses or compliances. The resulting matrix of elastic constants $\langle C\rangle$ (equation (A11)) is independent of the domain of averaging (i.e., stiffnesses/compliances) and therefore is a unique solution of the ODF averaging procedure. *Cholach* [2005] provides further details on the implementation of these calculations.

[65] **Acknowledgments.** This work was supported by Natural Science and Engineering Research Council of Canada and by the COURSE fund provided by the Alberta Energy Research Institute. D. Collis and C. D. Rokosh collected the SEM images from a shale core provided by R. Wong. The authors greatly appreciate the efforts of the Associate Editor K. Wang and the two reviewers, S. Ji and D. Okaya.

References

Aleksandrov, K. S., and L. A. Aizenberg (1966), Method of calculating physical constants of polycrystalline materials, *Dokl. Akad. Nauk SSSR*, *167*, 1028–1031.

Alexandrov, K. S., and T. V. Ryzhova (1961), Elastic properties of rock-forming minerals. II. Layered silicates, *Izv. Acad. Sci. USSR Geophys. Ser.*, Engl. Transl., *12*, 1165–1168.

Alkhalifah, T., and I. Tsvankin (1995), Velocity analysis for transversely isotropic media, *Geophysics*, *60*, 1550–1566.

Aplin, A. C., I. F. Matenaar, and B. van der Pluijm (2003), Influence of mechanical compaction and chemical diagenesis on the microfabric and fluid flow properties of Gulf of Mexico mudstones, *J. Geochem. Explor.*, *78–79*, 449–451.

Babuška, V., and M. Cara (1991), *Seismic Anisotropy in the Earth*, 232 pp., Springer, New York.

Backus, G. E. (1962), Long-wave elastic anisotropy produced by horizontal layering, *J. Geophys. Res.*, *67*(11), 4427–4440.

Backus, G. E. (1970), A geometrical picture of anisotropic elastic tensors, *Rev. Geophys.*, *8*(3), 633–671.

Banik, N. C. (1984), Velocity anisotropy of shales and depth estimation in the North Sea basin, *Geophysics*, *49*, 1411–1420.

Barruol, B., and D. Mainprice (1993), A quantitative evaluation of the contribution of crustal rocks to the shear wave splitting of teleseismic SKS waves, *Phys. Earth Planet. Inter.*, *78*, 281–300.

Berge, P. A., and J. G. Berryman (1995), Realizability of negative pore compressibility in poroelastic composites, *J. Appl. Mech.*, *62*, 1053–1062.

Brocher, T. M., and N. I. Christensen (1990), Seismic anisotropy due to preferred mineral orientations observed in shallow crustal rocks in southern Alaska, *Geology*, *18*, 737–740.

Bunge, H.-J. (1982), *Texture Analysis in Material Science*, 593 pp., Butterworths, London.

Bunge, H.-J., C. Esling, and J. Muller (1981), The influence of crustal and sample symmetries on the orientation distribution function of the crystalline materials, *Acta Crystallogr., Sect. A Cryst. Phys. Diffr. Theor. Gen. Crystallogr.*, *37*, 889–899.

Burlini, L., and D. M. Fountain (1993), Seismic anisotropy of metapelites from the Ivrea-Verbano zone and Serie dei Laghi (northern Italy), *Phys. Earth Planet. Inter.*, *78*, 301–317.

Carrion, P., J. Costa, J. E. Ferrer-Pinheiro, and M. Schoenberg (1992), Cross-borehole tomography in anisotropic media, *Geophysics*, *57*, 1194–1198.

Castagna, J. P., M. L. Batzle, and R. L. Eastwood (1985), Relationship between compressional-wave and shear-wave velocities in clastic silicate rocks, *Geophysics*, *50*, 571–581.

Chen, S. Z., et al. (2005), Petrology and mineralogy of PP3 ultramafic rocks in Sulu UHP belt and its significance, *Acta Pet. Sin.*, *21*, 369–380.

Cholach, P. Y. (2005), The elasticity of intrinsically anisotropic rocks, Ph.D. dissertation, 167 pp., Univ. of Alberta, Edmonton, Alberta, Canada.

Cholach, P. Y., J. B. Molyneux, and D. R. Schmitt (2005), Flin Flon belt seismic anisotropy: Elastic symmetry, heterogeneity, and shear wave splitting, *Can. J. Earth Sci.*, *42*, 533–544.

Chung, D. H., and W. R. Buessem (1967), The Voigt-Reuss-Hill approximation and elastic moduli of polycrystalline MgO, CaF_2, β-ZnS, ZnSe, and CdTe, *J. Appl. Phys.*, *38*, 2535–2540.

Comodi, P., and P. F. Zanazzi (1995), High-pressure structural study of muscovite, *Phys. Chem. Miner.*, *22*, 170–177.

Comodi, P., P. Fumagalli, M. Montagnoli, and P. F. Zanazzi (2004), A single-crystal study on the pressure behavior of phlogopite and petrological implications, *Am. Mineral.*, *89*, 647–653.

Deer, W. A., R. A. Howie, and J. Zussman (1964), *Rock-Forming Minerals*, vol. 3, *Sheet Silicates*, Pitman, London.

Domnesteanu, P., C. McCann, and J. Sothcott (2002), Velocity anisotropy and attenuation of shale in under- and overpressured conditions, *Geophys. Prospect.*, *50*, 487–503.

Ferrari, M., and G. C. Johnson (1988), The equilibrium properties of a 6 mm polycrystal exhibiting transverse isotropy, *J. Appl. Phys.*, *63*, 4460–4468.

Gassmann, F. (1964), Introduction to seismic travel time methods in anisotropic media, *Pure Appl. Geophys.*, *58*, 63–113.

Godfrey, N. J., N. I. Christensen, and D. A. Okaya (2000), Anisotropy of schists: Contribution of crustal anisotropy to active source seismic experiments and shear wave splitting observations, *J. Geophys. Res.*, *105*(B12), 27,991–28,007.

Godfrey, N. J., N. I. Christensen, and D. A. Okaya (2002), The effect of crustal anisotropy on reflector depth and velocity determination from wide-angle seismic data: A synthetic example based on South Island, New Zealand, *Tectonophysics*, *355*, 145–161.

Hashin, Z., and S. Shtrikman (1963), A variational approach to the theory of elastic behaviour of multiphase materials, *J. Mech. Phys. Solids*, *11*, 127–140.

Hazen, R. M., and L. W. Finger (1978), Crystal-structures compressibilities of layer minerals at high-pressure: 2. Phlogopite and chlorite, *Am. Mineral.*, *63*, 293–296.

Hearn, B. C. (2004), The Homestead kimberlite, central Montana, USA: Mineralogy, xenocrysts, and upper-mantle xenoliths, *Lithos*, *77*, 473–491.

Hill, R. (1952), The elastic behaviour of a crystalline aggregate, *Proc. Phys. Soc. London, Sect. A*, *65*, 349–354.

Ho, N.-C., D. R. Peacor, and B. A. van der Pluijm (1999), Preferred orientation of phyllosilicates in Gulf Coast mudstone and relation to the smectite-illite transformation, *Clays Clay Miner.*, *47*, 495–504.

Hornby, B. E. (1995), The elastic properties of shales, Ph.D. thesis, Univ. of Cambridge, Cambridge, U. K.
Hornby, B. E. (1998), Experimental laboratory determination of the dynamic elastic properties of wet, drained shales, *J. Geophys. Res.*, *103*(B12), 29,945–29,964.
Hornby, B. E., L. M. Schwartz, and J. A. Hudson (1994), Anisotropic effective-medium modeling of the elastic properties of shales, *Geophysics*, *59*, 1570–1583.
Israelachvili, J. N., N. A. Alcantar, N. Maeda, T. E. Mates, and M. Ruths (2004), Preparing contamination-free mica substrates for surface characterization, force measurements, and imaging, *Langmuir*, *20*, 3616–3622.
Jacob, G., H. J. Kisch, and B. A. van der Pluijm (2000), The relationship of phyllosilicate orientation, X-ray diffraction intensity ratios, and c/b fissility ratios in metasedimentary rocks of the Helvetic zone of the Swiss Alps and the Caledonides of Jaemtland, central western Sweden, *J. Struct. Geol.*, *22*, 245–258.
Jakobsen, M., and T. A. Johansen (2000), Anisotropic approximation for mudrocks: A seismic laboratory study, *Geophysics*, *65*, 1711–1725.
Jakobsen, M., J. A. Hudson, and T. A. Johansen (2003), T-matrix approach to shale acoustics, *Geophys. J. Int.*, *154*, 533–558.
Ji, S. C., and M. H. Salisbury (1993), Shear-wave velocities, anisotropy and splitting in high-grade mylonites, *Tectonophysics*, *221*, 453–473.
Ji, S., Q. Wang, and B. Xia (2003), *P*-wave velocities of polymineralic rocks: Comparison of theory and experiment and test of elastic mixture rules, *Tectonophysics*, *366*, 165–185.
Ji, S., Q. Wang, B. Xia, and D. Marcotte (2004), Mechanical properties of multiphase materials and rocks: A phenomenological approach using generalized means, *J. Struct. Geol.*, *26*, 1377–1390.
Johansen, T. A., B. O. Rudd, and M. Jakobsen (2004), Effect of grain scale alignment on seismic anisotropy and reflectivity of shales, *Geophys. Prospect.*, *52*, 133–149.
Johnston, J. E., and N. I. Christensen (1995), Seismic anisotropy of shales, *J. Geophys. Res.*, *100*(B4), 5991–6003.
Jolly, R. N. (1956), Investigation of shear waves, *Geophysics*, *21*, 905–938.
Jones, L. E. A., and H. F. Wang (1981), Ultrasonic velocities in Cretaceous shales from the Williston basin, *Geophysics*, *46*, 288–297.
Kaarsberg, E. A. (1959), Introductory studies of natural and artificial argillaceous aggregates by sound-propagation and X-ray diffraction methods, *J. Geol.*, *67*, 447–472.
Katahara, K. W. (1996), Clay mineral elastic properties, paper presented at SEG International Exposition and 66th Annual Meeting, Soc. of Explor. Geophys., Denver, Colo.
Kebaili, A., and D. R. Schmitt (1996), Velocity anisotropy observed in wellbore seismic arrivals: Combined effect of intrinsic properties and layering, *Geophysics*, *61*, 12–20.
Kern, H., and H.-R. Wenk (1990), Fabric-related velocity anisotropy and shear wave splitting in rocks from Santa Rosa Mylonite Zone, California, *J. Geophys. Res.*, *95*(B7), 11,213–11,223.
Kröner, E. (1958), Berechnung der elastischen Konstanten des Vielkristalls aus den Konstanten des Einkristalls, *Z. Phys. A Hadrons Nuclei*, *151*, 504–518.
Kröner, E. (1978), Self-consistent scheme and gradient disorder in polycrystal elasticity, *J. Phys. F Met. Phys.*, *8*, 2261–2267.
Kumazawa, M. (1969), The elastic constant of polycrystalline rocks and nonelastic behavior inherent to them, *J. Geophys. Res.*, *74*, 5311–5320.
Leaney, W. S., C. M. Sayers, and D. E. Miller (1999), Analysis of multi-azimuthal VSP data for anisotropy and AVO, *Geophysics*, *64*, 1172–1180.
Leslie, J. M., and D. C. Lawton (1999), A refraction-seismic field study to determine the anisotropic parameters of shales, *Geophysics*, *64*, 1247–1252.
Mah, M. (2005), Determination of the elastic constants of orthorhombic and transversely isotropic materials: Experimental application to a kerogen rich rock, Ph.D. dissertation, Univ. of Alberta, Edmonton, Alberta, Canada.
Mainprice, D., and M. Humbert (1994), Methods of calculating petrophysical properties from lattice preferred orientation data, *Surv. Geophys.*, *15*, 575–592.
Marion, D., A. Nur, and D. Han (1992), Compressional velocity and porosity in sand- clay mixtures, *Geophysics*, *57*, 554–563.
Matthies, S., and M. Humbert (1993), The realization of the concept of a geometric mean for calculating physical constants of polycrystalline materials, *Phys. Status Solidi B*, *177*, K47–K50.
McDonough, D. T., and D. M. Fountain (1993), *P*-wave anisotropy of mylonitic and infrastructural rocks from a Cordilleran core complex: The Ruby-East Humboldt Range, Nevada, *Phys. Earth. Planet. Inter.*, *78*, 319–336.
Miller, D. E., S. Leaney, and W. H. Borland (1994), An in situ estimation of anisotropic elastic moduli for a submarine shale, *J. Geophys. Res.*, *99*(B11), 21,659–21,665.
Morawiec, A. (1989), Calculation of polycrystal elastic constants from single-crystal data, *Phys. Status Solidi B*, *154*, 535–541.
Morris, P. R. (1970), Elastic constants of polycrystals, *Int. J. Eng. Sci.*, *8*, 49–61.
Morse, P. M., and H. Feshbach (1953), *Methods of Theoretical Physics*, McGraw-Hill, New York.
Musgrave, M. J. P. (1970), *Crystal Acoustics: Introduction to the Study of Elastic Wave and Vibrations in Crystals*, 288 pp., Holden-Day, Boca Raton, Fla.
Nishizawa, O., and T. Yoshino (2001), Seismic velocity anisotropy in mica-rich rocks: An inclusion model, *Geophys. J. Int.*, *145*, 19–32.
Nye, J. F. (1990), *Physical Properties of Crystals*, 329 pp., Oxford Univ. Press, New York.
O'Brien, D. K., H.-R. Wenk, L. Ratscbacher, and Z. You (1987), Preferred orientation of phyllosilicates in phyllonities and ultramylonites, *J. Struct. Geol.*, *9*, 719–730.
Oertel, G. (1983), The relationship of strain and preferred orientation of phyllosilicate grains in rocks: A review, *Tectonophysics*, *100*, 413–447.
Okaya, D. A., and N. I. Christensen (2002), Anisotropic effects of non-axial seismic wave propagation in foliated crustal rocks, *Geophys. Res. Lett.*, *29*(11), 1507, doi:10.1029/2001GL014285.
Okaya, D. A., and T. V. McEvilly (2003), Elastic wave propagation in anisotropic crustal material possessing arbitrary internal tilt, *Geophys. J. Int.*, *153*, 344–358.
Okaya, D., W. Rabbel, T. Beilecke, and J. Hasenclever (2004), *P* wave material anisotropy of a tectono-metamorphic terrane: An active source seismic experiment at the KTB super-deep drill hole, southeast Germany, *Geophys. Res. Lett.*, *31*, L24620, doi:10.1029/2004GL020855.
Ono, N. (1992), Physical relevance of physical elasticity theories, *Scr. Metall. Mater.*, *27*, 1379–1384.
Pavese, A., G. Ferraris, V. Pischedda, and R. Ibberson (1999), Tetrahedral order in phengite 2M(1) upon heating, from powder neutron diffraction, and thermodynamic consequences, *Eur. J. Mineral.*, *2*, 309–320.
Pavese, A., D. Levy, N. Curetti, V. Diella, P. Fumagalli, and A. Sani (2003), Equation of state and compressibility of phlogopite by in-situ high-pressure X-ray powder diffraction, *Eur. J. Mineral.*, *15*, 455–463.
Podio, A. L., A. R. Gregory, and M. E. Grey (1968), Dynamic properties of dry and saturated Green River shale under stress, *Soc. Pet. Eng. J.*, *8*, 389–404.
Prasad, M., M. Kopycinska, U. Rabe, and W. Arnold (2002), Measurement of Young's modulus of clay minerals using atomic force acoustic microscopy, *Geophys. Res. Lett.*, *29*(8), 1172, doi:10.1029/2001GL014054.
Pulford, A., M. Savage, and T. Stern (2003), Absent anisotropy: The paradox of the Southern Alps orogen, *Geophys. Res. Lett.*, *30*(20), 2051, doi:10.1029/2003GL017758.
Purton, J. A., N. I. Allan, and J. D. Blundy (1997), Impurity cations in the bulk and the {001} surface of muscovite: An atomistic simulation study, *J. Mater. Chem.*, *7*, 1947–1951.
Putnis, A. (1992), *Introduction to Mineral Sciences*, 457 pp., Cambridge Univ. Press, New York.
Reuss, A. (1929), Berechnung der Flieβgrenze von Mischkristallen aufgrund der Plastizitätsbedingung für Einkristalle, *Z. Angew. Math. Mech.*, *9*, 49–58.
Roe, R.-J. (1965), Description of crystallite orientation in polycrystalline materials. III. General solution to pole inversion, *J. Appl. Phys.*, *36*, 2024–2031.
Sayers, C. M. (1993), Anelliptic approximations for shales, *J. Seismol. Explor.*, *2*, 319–331.
Sayers, C. M. (1994), The elastic anisotropy of shales, *J. Geophys. Res.*, *99*(B1), 767–774.
Sayers, C. M. (1995), Simplified anisotropy parameters for transversely isotropic sedimentary rocks, *Geophysics*, *60*, 1933–1935.
Sayers, C. M. (1999), Stress-dependent seismic anisotropy of shales, *Geophysics*, *64*, 93–98.
Sayers, C. M. (2005), Seismic anisotropy of shales, *Geophys. Prospect.*, *53*, 667–676.
Schoenberg, M., and F. Muir (1989), A calculus for finely layered anisotropic media, *Geophysics*, *54*, 581–589.
Schoenberg, M., F. Muir, and C. Sayers (1996), Introducing ANNIE: A simple three-parameter anisotropic velocity model for shales, *J. Seismol. Explor.*, *5*, 35–49.
Shapiro, N. M., M. H. Ritzwoller, P. Molnar, and V. Levin (2004), Thinning and flow of Tibetan crust constrainted by seismic anisotropy, *Science*, *305*, 233–236.
Sheng, P., and A. J. Callegari (1984), Differential effective medium theory of sedimentary rocks, *Appl. Phys. Lett.*, *44*, 738–740.
Simmons, G., and H. Wang (1971), *Single Crystal Elastic Constants and Calculated Aggregate Properties: A Handbook*, 370 pp., MIT Press, Cambridge, Mass.

Sintubin, M. (1994a), Clay fabrics in relation to the burial history of shales, *Sedimentology*, *41*(6), 1161–1169.
Sintubin, M. (1994b), Phyllosilicate preferred orientation in relation to strain path determination in the lower Paleozoic Stavelot-Venn Massif (Ardennes, Belgium), *Tectonophysics*, *237*, 215–231.
Sintubin, M., H.-R. Wenk, and D. S. Phillips (1995), Texture development in platy materials: Comparison of Bi2223 aggregates with phyllosilicate fabrics, *Mater. Sci. Eng. A*, *202*, 157–171.
Smyth, J. R., S. D. Jacobsen, R. J. Swope, R. J. Angel, T. Arlt, K. Domanik, and J. R. Holloway (2000), Crystal structures and compressibilities of synthetic 2M(1) and 3T phengite micas, *Eur. J. Mineral.*, *12*, 955–963.
Sudo, A., and Y. Tatsumi (1990), Phlogopite and K-amphibole in the upper mantle: Implication for magma genesis in subduction zones, *Geophys. Res. Lett.*, *17*, 29–32.
Takanashi, M., O. Nishizawa, K. Kanagawa, and K. Yasunaga (2001), Laboratory measurements of elastic anisotropy parameters for the exposed crustal rocks from the Hidaka Metamorphic Belt, central Hokkaido, Japan, *Geophys. J. Int.*, *145*, 33–47.
Thomsen, L. (1972), Elasticity of polycrystals and rocks, *J. Geophys. Res.*, *77*(2), 315–327.
Thomsen, L. (1986), Weak elastic anisotropy, *Geophysics*, *51*, 1954–1966.
Tosaya, C. A. (1982), Acoustic properties of clay-bearing rocks, Ph.D. thesis, Stanford Univ., Stanford, Calif.
Tronnes, R. G. (2002), Stability range and decomposition of potassic richterite and phlogopite end members at 5–15 GPa, *Mineral. Petrol.*, *74*, 129–148.
Tsvankin, I., and L. Thomsen (1994), Non-hyperbolic reflection moveout in anisotropic media, *Geophysics*, *59*, 1290–1304.
Ullemeyer, K., G. Braun, M. Dahms, J. H. Kruhl, N. O. Olesen, and S. Siegesmund (2000), Texture analysis of a muscovite-bearing quartzite: A comparison of some currently used techniques, *J. Struct. Geol.*, *22*, 1541–1557.
Vanorio, T., M. Prasad, and A. Nur (2003), Elastic properties of dry clay mineral aggregates, suspensions and sandstones, *Geophys. J. Int.*, *155*, 319–326.
van Roermund, H. L. M., D. A. Carswell, and M. R. Drury (2002), Microdiamonds in a megacrystic garnet websterite pod from Bardane on the island of Fjortoft, western Norway: Evidence for diamond formation in mantle rocks during deep continental subduction, *Geology*, *30*, 959–962.
Vaughan, M. T., and S. Guggenheim (1986), Elasticity of muscovite and its relationship to crystal structure, *J. Geophys. Res.*, *91*(B5), 4657–4664.
Vergne, R. M., G. Wittlinger, V. Farra, and H. P. Su (2003), Evidence for upper crustal anisotropy in the Songpan-Ganze (northeastern Tibet) terrane, *Geophys. Res. Lett.*, *30*(11), 1552, doi:10.1029/2002GL016847.
Vernik, L. (1993), Microcrack-induced versus intrinsic elastic anisotropy in mature HC-source shales, *Geophysics*, *58*, 1703–1706.
Vernik, L., and X. Liu (1997), Velocity anisotropy in shales: A petrophysical study, *Geophysics*, *62*, 521–532.
Vernik, L., and A. Nur (1992), Ultrasonic velocity and anisotropy of hydrocarbon source rocks, *Geophysics*, *57*, 727–735.
Vestrum, R. W., D. C. Lawton, and R. Schmid (1999), Imaging structures below dipping TI media, *Geophysics*, *64*, 1239–1246.
Viglin, A. S. (1960), A quantitative measure of the texture of a polycrystalline material: Texture function, *Sov. Phys. Solid State*, *2*, 2195–2207.
Voigt, W. (1928), *Lehrbuch der Kristallphysik*, Teubner-Verlag, Leipzig, Germany.
Wang, Z. (2002), Seismic anisotropy in sedimentary rocks, part 2: Laboratory data, *Geophysics*, *67*, 1423–1440.
Wang, Z. Z., H. Wang, and M. E. Cates (1998), Elastic properties of solid clays, paper presented at SEG 68th Annual Meeting, Soc. of Explor. Geophys., New Orleans, La.
Watt, P. J., G. F. Davies, and R. J. O′Connell (1976), The elastic properties of composite materials, *Rev. Geophys.*, *14*, 541–563.
Weiss, T., S. Siegesmund, W. Rabbel, T. Bohlen, and M. Pohl (1999), Seismic velocities and anisotropy of the lower continental crust: A review, *Pure Appl. Geophys.*, *156*, 97–122.
White, J. E., L. Martineau-Nicoletis, and C. Monash (1983), Measured anisotropy in Pierre shale, *Geophys. Prospect.*, *31*, 709–725.
Winterstein, D. F., and B. N. P. Paulsson (1990), Velocity anisotropy in shale determined from crosshole seismic and vertical seismic profile data, *Geophysics*, *55*, 470–479.

P. Y. Cholach, BP Canada Energy Company, 240 4th Avenue S. W., Calgary, AB, Canada T2P 2H8.
D. R. Schmitt, Institute for Geophysical Research, Dept. of Physics, Mailstop 615, University of Alberta, Edmonton, AB, Canada T6G 2G7. (doug@phys.ualberta.ca)